Surface protection
of optical microfibres
for caesium spectroscopy

von

Jan Edgar Hartung

Diplomarbeit in Physik

angefertigt im
Institut für Angewandte Physik

vorgelegt der
Mathematisch-Naturwissenschaftlichen Fakultät
der Rheinischen Friedrich-Wilhelms-Universität Bonn

im Juli 2012

Referent: Prof. Dr. D. Meschede
Korreferent: Prof. Dr. M. Sokolowski

Contents

Introduction

In this thesis I present experiments done with optical fibres tapered down to submicrometre diameters. In such an optical microfibre, OMF, the light is strongly confined over a large length with a strong evanescent field propagating outside of the OMF. With this high light intensity in the surrounding medium of the OMF over a length of several millimetres, OMFs offer excellent conditions for light-matter interaction experiments.

Linear absorption spectroscopy of hot caesium vapour using OMFs has already been done in our group [1]. The goal of my work was to investigate the possibilities of further spectroscopic methods.

After presenting the considerations about pump - probe spectroscopy of caesium vapour using OMFs, I will introduce the optical setup I built. It offers the possibility for saturated absorption and polarisation spectroscopy using OMFs with a great flexibility.

In first experiments the setup proofed to work, but transmission losses due to chemical reactions of the caesium with the surface of the OMFs prevented further investigations.

To overcome this problem, the surface of the OMF had to be protected. I will present the surface passivation method which fulfils all of our demands and the developed treatment procedure of an OMF.

This treatment procedure can now be applied and an OMF with a chemically passivated surface can be connected to the ready to use optical setup for pump - probe spectroscopy of hot atmoic caesium vapour.

Introduction

1 Optical microfibres

Optical microfibres (OMFs) are circular, dielectric optical waveguides with a diameter on the order of one micrometre. Their optical properties will be presented in part one of this chapter, followed by their fabrication process in part two. I will then introduce the chemical surface properties of OMFs in the final part three, since these properties are important for the understanding of the behaviour of OMFs in chemical reactive environments, such as hot caesium vapour.

1.1 Principle of operation

In figure 1.1a an OMF is sketched. A section of an unprocessed optical fibre is followed by the down-taper, the micrometre waist, the up-taper and a second unprocessed optical fibre section.

The OMFs used in this work are made from bare optical step-index single-mode fibres with a germanium (Ge) doped fused silica (SiO_2) core and a surrounding fused silica cladding. The doping in the core increases the refractive index of the fused silica by 0.3 % to 0.4 % so that light in the core is guided along the fibre axis by total internal reflection at the core-cladding interface. The fundamental mode propagates mainly inside the core, with the evanescent field reaching into the cladding being of short spatial extension and low intensity (figure 1.1.b).

In the down-taper, the diameter of the fibre and the core decreases. The guiding of the core gets weaker and the light starts to expand into the cladding, in which it is guided by total internal reflection at the cladding-surrounding medium interface.

In the waist of an OMF with a cladding diameter of about one micrometre, the diameter of the core has reached a few tens of nanometres, so that its guidance can be neglected. The light is guided by total internal reflection at the cladding-surrounding medium interface with a large refractive index step, leading to a strong evanescent field around the waist of the OMF (figure 1.1c). With the intensity increasing at a submicrometre diameter waist up to two orders of magnitude and up to 50 % of the light intensity propagating outside of the fibre, OMFs are excellent tools for light-matter interaction experiments.

In the up-taper, the mode conversion of core-guided to cladding-guided modes is reversed.
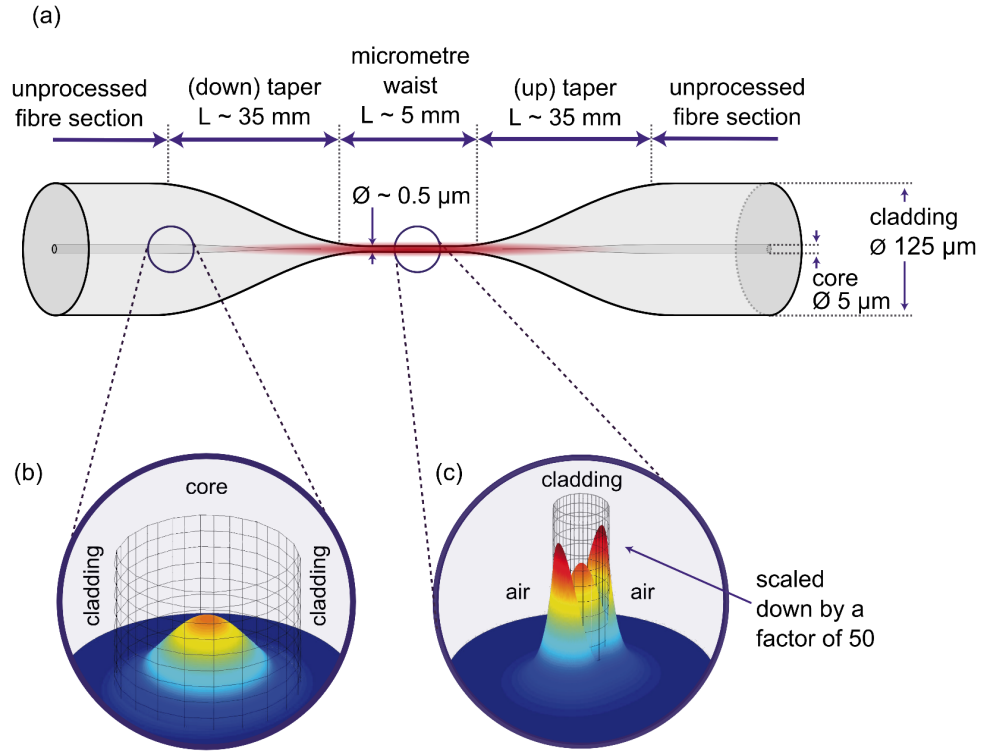
(a)

Figure 1.1: (a) Schematic Sketch of an OMF, (b) intensity distribution of a quasi-linearly polarised fundamental mode in an unprocessed single-mode fibre and (c) an OMF in air. *Taken from* [2]

For a maximum transmission through an OMF, coupling into higher, not guided modes at the tapers has to be prevented. This adiabaticity is achieved by shallow slopes of the tapers with angles of a few milliradians [3][2].

At a given wavelength, the diameter of the waist determines the intensity distribution of the light and, therefore, the amount of light propagating in the surrounding medium [2]. For a sufficient light-matter interaction in caesium vapour, a waist diameter of about 0.4 µm is needed [6].

1.2 Fabrication

In figure 1.2 the fabrication process of an OMF using the flame-brushing technique [6][3] is sketched. The single-mode fibres are fixed to translation stages and pulled apart while a moving oxygen-hydrogen burner heats the fibre to become less viscous. The movements of the translation stages and the burner determine the shape of the tapers, the length and the diameter of the waist [6]. For caesium spectroscopy adiabatic tapers are needed for maximum transmission [4][5]
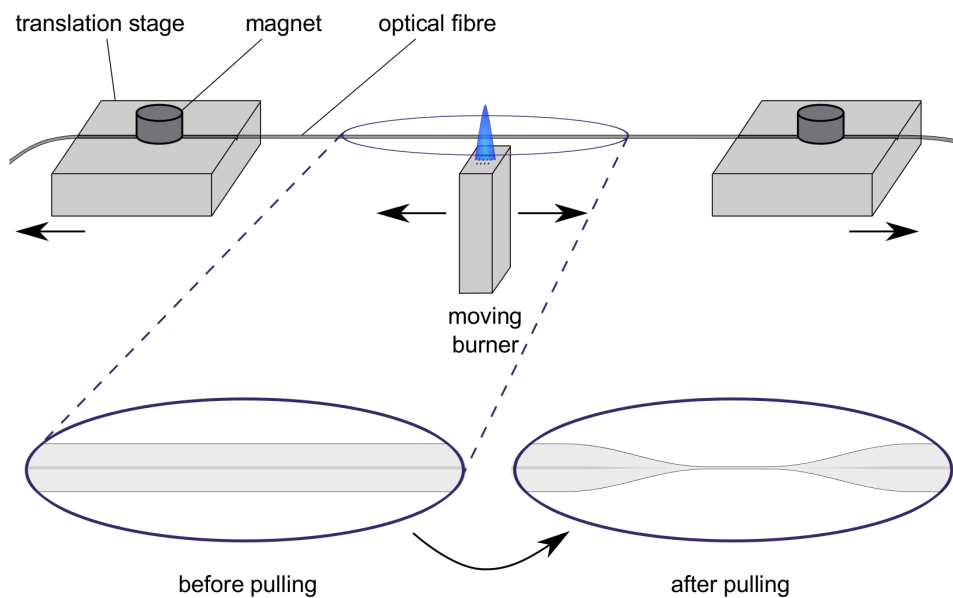
Figure 1.2: Pulling process of an OMF. *Taken from* [2]

After the pulling process the OMF is fixed to a fibre holder made of an aluminium alloy with the help of UV curing glue (figure 1.3). Then an aluminium cover is screwed to the holder to protect the OMF against mechanical stress and dust. The holder has threads on both sides for stable mounting.

Straightening the OMF before fixing it minimises the oscillation of the waist and reduces the risk of mechanical damage. But the heating of the OMF and the holder requires a destretching of the fibre.

Figure 1.3: Cover for protection and the fibre holder with an OMF glued to it. *Taken from* [1]

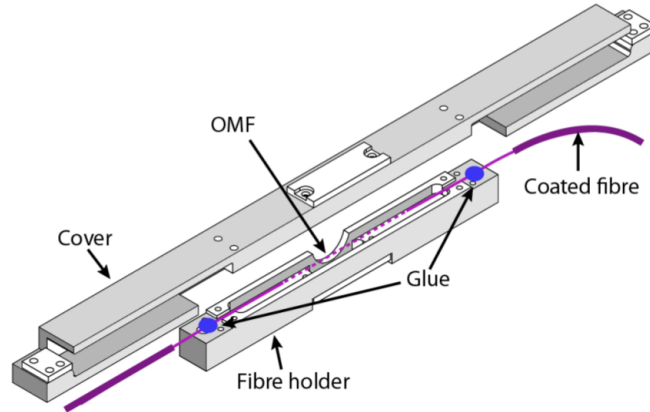The difference of the thermal expansion of the length of the holder, Δl_{holder}, and the OMF, Δl_{OMF}, is estimated by

$$\Delta l = \Delta l_{holder} - \Delta l_{OMF} \approx l_0 \cdot \alpha_{al} \cdot \Delta T - l_0 \cdot \alpha_{fs} \cdot \Delta T \approx 250 \mu m,$$

taken the thermal expansion coefficients of fused silica $\alpha_{fs} = 0.6 \cdot 10^{-6} K^{-1}$ for the OMF and of aluminium $\alpha_{al} = 23.2 \cdot 10^{-6} K^{-1}$ for the aluminium alloy of the holder, heating by $\Delta T = 100 \, K$, and the initial length of the fibre between the gluing points $l_0 = 11 \, cm$.

Although the OMF can be stretched by this length without ripping, it should be avoided. The stretching leads to a decrease of the diameters mainly of the waist and the thin taper parts and thus to a change of the optical properties of the OMF. Also, the risk of producing cracks in the silica is increased by stretching the OMF.

Therefore, OMFs used in hot caesium vapour have to be destretched by a few hundred micrometres.

1.3 Chemical properties of the silica surface

The cladding of the optical fibres used for pulling our OMF is made of fused silica, so the surface of our OMF is expected to have the same chemical properties as fused silica.

Silica, an amorphous SiO_2, mainly consists of siloxane groups ($\equiv$Si-O-Si$\equiv$). These groups are as chemically stable and not reactive as the silica itself, also as surface groups (figure 1.4a) [7].
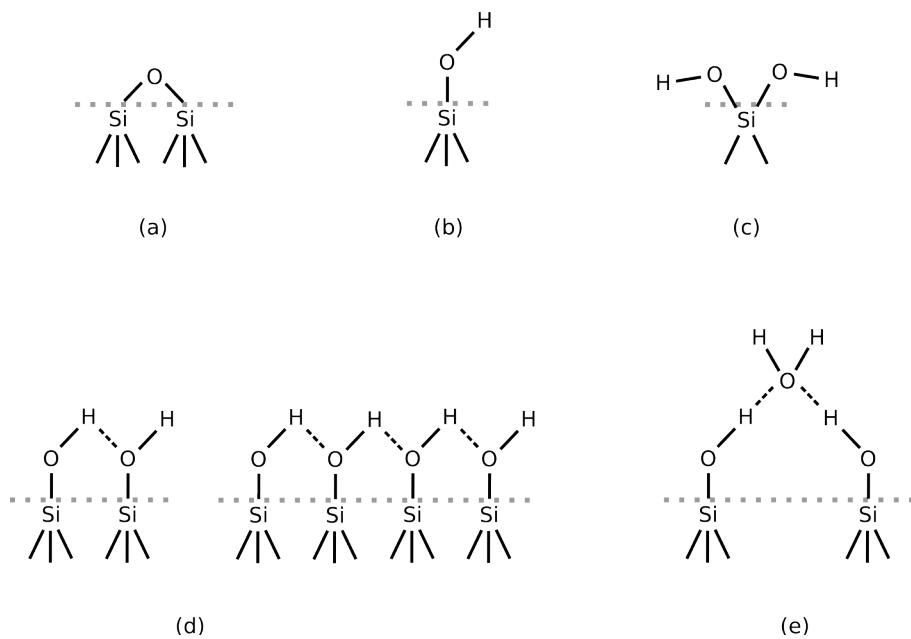
Figure 1.4: Surface groups of silica: (a) siloxane group, (b) isolated silanol, (c) silanol with two hydroxyl groups, (d) silanols close enough for the hydroxyl groups to form hydrogen bridges, (e) silanols bound to a water molecule with hydrogen bridges. Water molecules can bind to all shown silanols via hydrogen bridges and form a strongly bound layer. [7]

But for silica being amorphous, it has randomly broken crystal structures, resulting in open, reactive or dangling bonds throughout the material. At the surface of silica, silanol groups ($\equiv$Si-OH) are formed at these bonds in air (figure 1.4b-e) [7].

The hydroxyl group (-OH) makes the silanol group very reactive. The

silanol groups are hydrophilic, leading to the formation of water layers with the number of molecular layers depending on the humidity of the surrounding medium. Organic and inorganic Molecules and atoms can bind physically, chemically or electrostatically to the water molecules or the silanol groups themselves under ambient conditions [7][8]. In contrast, a fully dehydroxylated silica surface (only siloxane groups, no silanol groups) is hydrophobic [7].

The average density of silicium atoms at the surface of silica is about five per square nanometre [7][9][10]. At a fully hydroxylated silica surface (only silanol groups, no siloxane groups), all silicium atoms form silanol groups. Depending on the history of a specific silica sample, a certain amount of these silanol groups may have condensed to siloxane groups [7].

For fused silica, the average density of surface silanol groups is about one per square nanometre [11][12][13], so that that the average density of surface siloxane groups is about two per square nanometre. In contrast to other silica types, the silanol group density of fused silica can be influenced only to a very minor degree [13] and thus can be taken as approximately constant.

2 Caesium spectroscopy

Spectroscopy of an atomic caesium vapour can give information about the actual status of the contributing caesium atoms, like their temperature, velocity distribution, anisotropy and shifted energy levels, and can lead to qualitative and quantitative descriptions of influencing factors like external fields, surfaces in or around the vapour and the properties of the light field.

The spectroscopy methods described in this chapter are used with caesium in a vapour cell to obtain reference spectra. Using an optical microfibre in hot caesium vapour, these methods offer the possibility to study, for example, transit time and surface effects.

I will, furthermore, describe a possible method to determine spectroscopically the polarisation of the light at the waist of an OMF.

2.1 Caesium D2 transition

I have chosen to use the D2 transition of caesium for spectroscopy, this is the transition from the $6^2S_{1/2}$ to the $6^2P_{3/2}$ state with a corresponding wavelength of 852.35 nm. The hyperfine levels of these states have different total angular momenta with F being their quantum number (figure 2.1). The selection rules for allowed transitions between these levels require $\Delta F = 0, \pm 1$.

I used the transitions from the $F = 3$ ground state to the allowed $F' = 2, 3, 4$ excited states, because the saturated absorption spectra of this transition group have some characteristics needed for the planned caesium spectroscopy with OMFs (see section 2.4). In the following text, F is the quantum number of the total angular momentum of a ground state and F' the quantum number of the total angular momentum of an excited state.
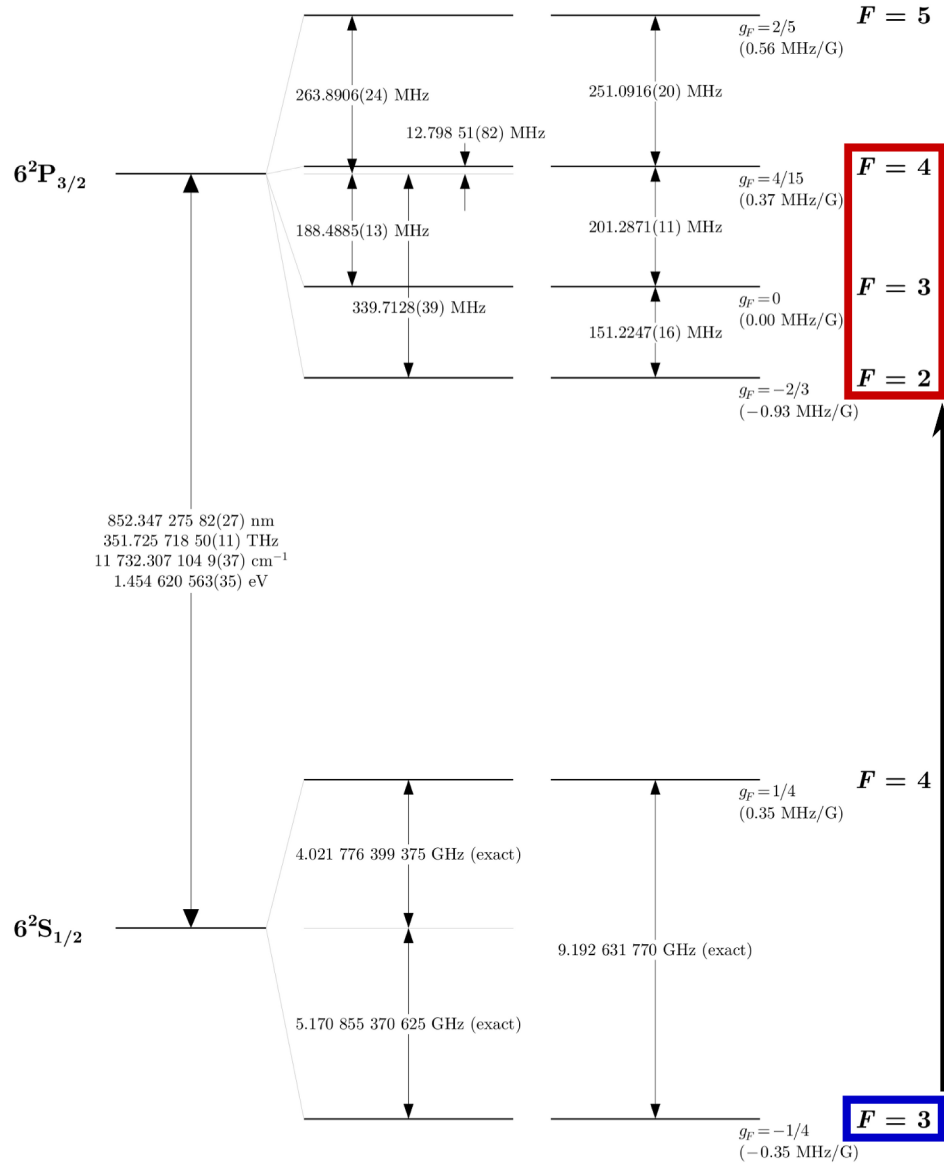
Figure 2.1: Caesium D2 transition hyperfine structure, the used excitations are marked. *Reproduced from* [14]

2.2 Linear absorption spectroscopy

A probe beam, with its frequency being scanned around the $F = 3 \rightarrow F' = 2, 3, 4$ transition frequencies and directed through a caesium vapour, gets absorbed by the atoms at the three corresponding transition frequencies. These absorption lines are broadened due to at least two effects.

First, the finite lifetime of an excited state gives a broadening with a Lorentzian profile. The full width at half maximum (FWHM) is the natural linewidth of 5.2 MHz.

Second, due to the thermal velocity of the atoms the Doppler effect is dominant, leading to the Doppler broadening of the absorption lines (figure 2.2).

Let $v_{\parallel}$ be the velocity component of an atom parallel to the probe beam axis, with a positive sign for pointing in the same direction as the propagation direction of the probe beam and a negative one for the opposite one. Then the frequency v of the light seen by the atom has a Doppler shift from the frequency v_0 of the light in the rest frame of the light source (c = velocity of light):

$$v = v_0 \cdot \left(1 - \frac{v_{\parallel}}{c}\right) \ .$$

This leads to the Doppler broadening of the absorption lines, because also light with v_0 being not a transition frequency can excite atoms with v at a transition frequency. The Doppler broadened absorption line has a Gaussian profile with a FWHM Δv_D of [15]

$$\Delta v_D = 7.16 \cdot 10^{-7} \cdot v_0 \cdot \sqrt{\frac{T_{Cs}}{M_{Cs}}} \ ,$$

with T_{Cs} = temperature of the caesium atoms in Kelvin and M_{Cs} = the molar mass of caesium, $M_{Cs} \approx 132.91 \, g/mol$. Taking $v_0 \approx 351.73 \, THz$ (see figure 2.1), one gets for the FWHM at 20 °C $\Delta v (20 \, °C) \approx 373.9 \, MHz$ and for the FWHM at 80 °C $\Delta v (80 \, °C) \approx 410.4 \, MHz$.

The three transitions of caesium atoms from the $F = 3$ ground state are so close to each other that the Doppler broadening, even at room temperature, gives a single, overall absorption dip (figure 2.2).
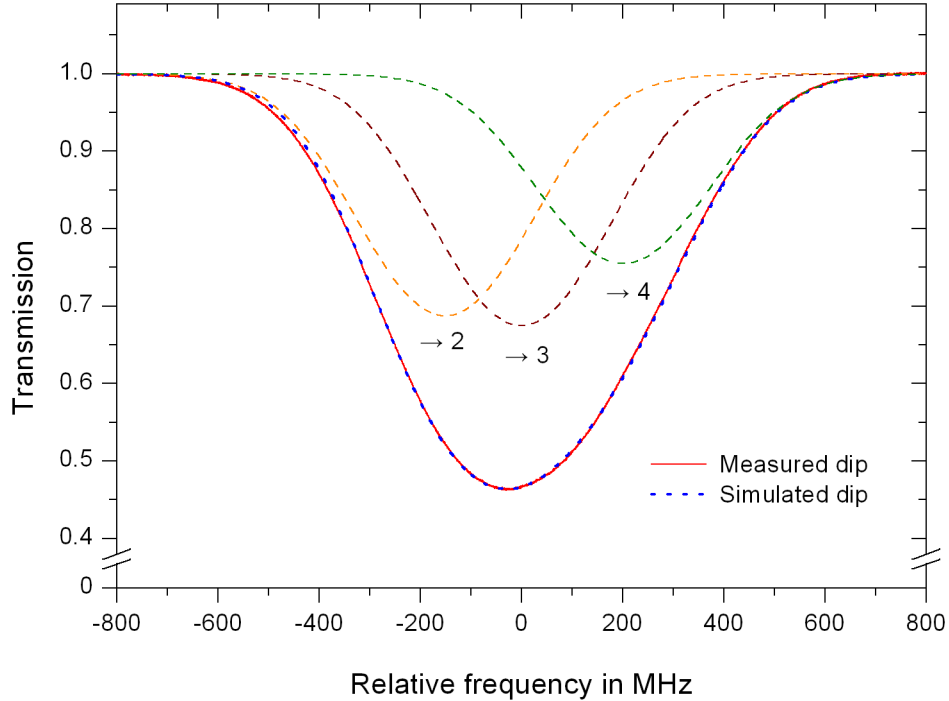
Figure 2.2: Linear absorption dip around the $F = 3 \rightarrow F' = 2, 3, 4$ D2 transitions of caesium. Solid line: Linear absorption spectrum from my reference spectroscopy setup. Dashed lines: Simulated absorption dips of the single $F = 3 \rightarrow F' = 2, 3, 4$ transitions ($= e^{-\text{Voigt profiles}}$) considering a natural linewidth of 5.2 MHz and a Doppler broadening at 20 °C of 373.9 MHz (FWHM). The dips are simulated to represent a dip depth of the simulated overall linear absorption dip ($= e^{-\Sigma \text{Voigt profiles}}$, dotted line) matching the dip depth of the experimental one (solid line). The $F = 3 \rightarrow F' = 3$ transition frequency is taken as zero.

Using an OMF for linear absorption spectroscopy in hot caesium vapour the Doppler broadening of the linear absorption dip can be taken to determine the temperature of the caesium vapour the OMF is exposed to [1].

Another important broadening effect for OMFs in hot caesium vapour is due to the short time of flight of an atom through the light field of the OMF. The transit time broadening becomes important when the time the atoms

stay in the light field is in the order of the natural lifetime of the excited states [16].

At vapour temperatures of a few hundred degrees caesium atoms have an average thermal velocity of a few hundred meters per second. With laser beam diameters in the order of one millimetre, an atom is several microseconds inside the light field while flying through the beam, which is long compared to the natural lifetime of a $6^2P_{3/2}$ state of about 30.4 ns [14].

The diameter of the light field around an OMF is in the order of one micrometre [spillane, fabian, uli, warken], so that an atom is several nanoseconds inside the light field, which is short compared to their natural lifetime. Therefore, the transit time broadening gives a relevant contribution to the broadening of the absorption lines of about 100 MHz [17][1].

2.3 Saturated absorption spectroscopy

In saturated absorption spectroscopy, the probe beam is spatially overlapped along its propagation axis with a counterpropagating pump beam at the same frequency, but with a higher intensity. Pump and probe beam interact resonantly with the same caesium atoms only if these are in certain velocity groups.

Atoms with no velocity component along the beam axis see the same frequency of the pump and the probe beam. At a transition frequency, the pump and the probe beam depopulate the ground state of these atoms by exciting them, leading to a decreased absorption of the probe beam and a peak in the transmission, or, equivalently, a dip in the absorption, the Lamb dip. Because only atoms with zero velocity along the beam axes contribute to these Lamb dips, they are not Doppler broadened. This leads to narrow peaks within the overall absorption dip, see figure 2.3.

Exactly in the frequency middle of two transitions the so called crossover peaks occur, with two velocity groups of the atoms contributing to them. An atom, which has a velocity component along the beam axes so that the Doppler shifted frequency of the pump beam equals the transition frequency of the higher transition, will see the frequency of the probe beam Doppler shifted to the frequency of the lower transition, and vice versa for atoms with an opposite velocity component along the beam axes. The probe beam sees the hole burnt into the populations of the excitable atoms, leading to a decreased absorption and the crossover peaks. Because only atoms with a distinct velocity component along the beam axis contribute to these absorption dips, the crossover peaks are also Doppler free (figure 2.3).
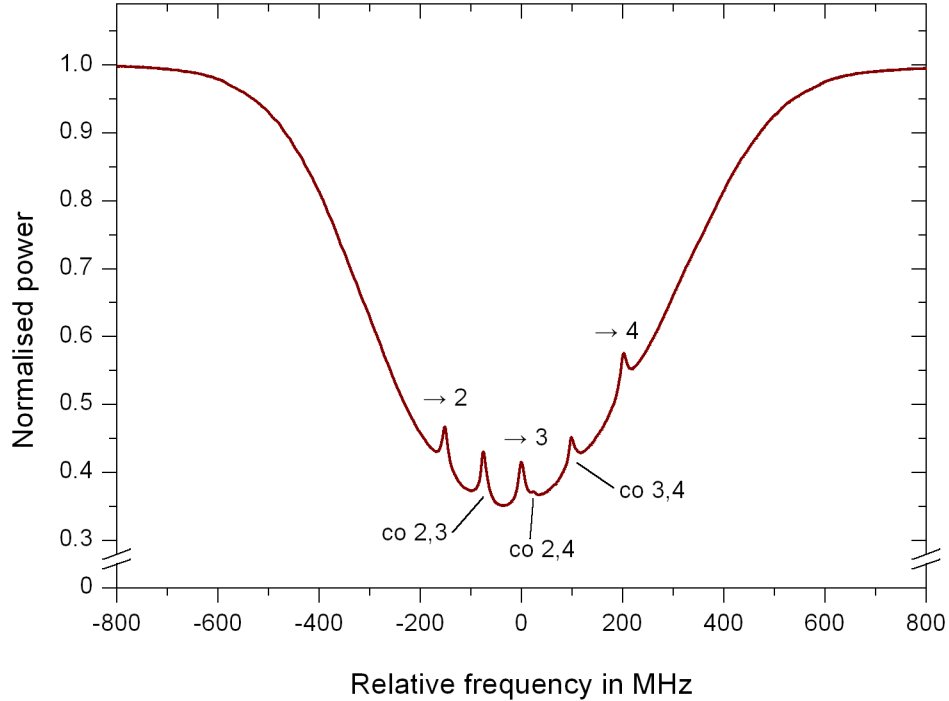
Figure 2.3: Saturated absorption spectrum from my reference spectroscopy setup with σ^+ - polarised pump and probe beam, $I_{pump}/I_{probe} \approx 4$, $T \approx 20\,°C$. The Lamb dips belonging to $F'=2, 3, 4$ are indicated by $\rightarrow$ 2, 3, 4; co x,y stands for the crossover peak between F' = x and F' = y. The $F=3 \rightarrow F'=3$ transition frequency is taken as zero.

In saturated absorption spectra of caesium vapour using OMFs, the transit time broadening (see section 2.2) contributes dominantly to the dip shapes [17]. Analysing the transit time broadening using an OMF gives information about the velocity distribution of the caesium atoms in the light field around the waist.

Caesium atoms with a mean velocity determined by the temperature are only several nanoseconds in the light field around an OMF (see section 2.2). But slow atoms stay longer in the field and their absorption lines are less transit time broadened. Due to their longer time in the light field, slow atoms contribute more to the absorption than fast ones. This additional velocity selection might be observable in the dip shapes [16].

Due to the presence of the waist, the van der Waals shift of the energy levels of the caesium atoms could be observable in the spectra [18].

2.4 Optical pumping

With laser beam diameters in the order of one millimetre, caesium atoms stay several microseconds in the light field (see section 2.2). With a lifetime of the excited states of about 30.4 ns [14], a single caesium atom is excited a few hundred times during this exposure to the light.

Due to the selection rules, the $F'=2$ excited state can only decay to the $F=3$ ground state, but the $F'=3, 4$ excited states can also decay to the $F=4$ ground state, which can not be excited by a laser scanning around the $F=3 \rightarrow F'=2, 3, 4$ transitions.

With no external magnetic field, the magnetic sublevels m_F belonging to the states ($m_F = -F, -F+1, \ldots, 0, \ldots, F-1, F$) are energetically degenerate, for a transition $\Delta m_F = 0, \pm 1$ is required.

The polarisation of the light exciting an atom determines Δm_F. For linearly or π - polarised light $\Delta m_F = 0$, right handed circularly or σ^+ - polarised light $\Delta m_F = +1$ and for left handed circularly or σ^- - polarised light $\Delta m_F = -1$. For the decay of an excited state, the probabilities for Δm_F being $0, \pm 1$ depend on F, m_F and are given in [19]. Atoms can end in an m_F ground state which can not be excited by light with a certain polarisation (dark state). For example, atoms in the $F=3, m_F = +3$ can not be excited to the $F'=2, 3$ states by a probe beam with σ^+ - polarisation.

Due to the numerous excitations of a caesium atom in the light beam, the F, m_F levels can be populated or depopulated by the pump and the probe beam. The effectiveness of these optical pumping processes depends on the intensity of the pump and the probe beam and on their polarisation [19].

The optically pumped caesium atoms leaving the light field usually thermalise at the walls surrounding the vapour or due to collisions, giving then an equal distribution among the ground states and the m_F levels.

The strong dependence of the actual dip strengths and shapes of a saturated absorption spectrum on the polarisation of the pump and the probe beam [19] could be reproduced in my reference spectroscopy setup (figure 2.4). At the crossover peak between the $F=3 \rightarrow F'=2$ and $F=3 \rightarrow F'=3$ transitions there is even a sign reversal of the absorption dip, which means an increased absorption relative to the Doppler broadened background, for

both pump and probe beam linearly polarised with their polarisation axes parallelly oriented. The occurrence of this sign reversed dip is a verification of the magnetic isolation of the caesium vapour cell [19], see section 3.1.1.
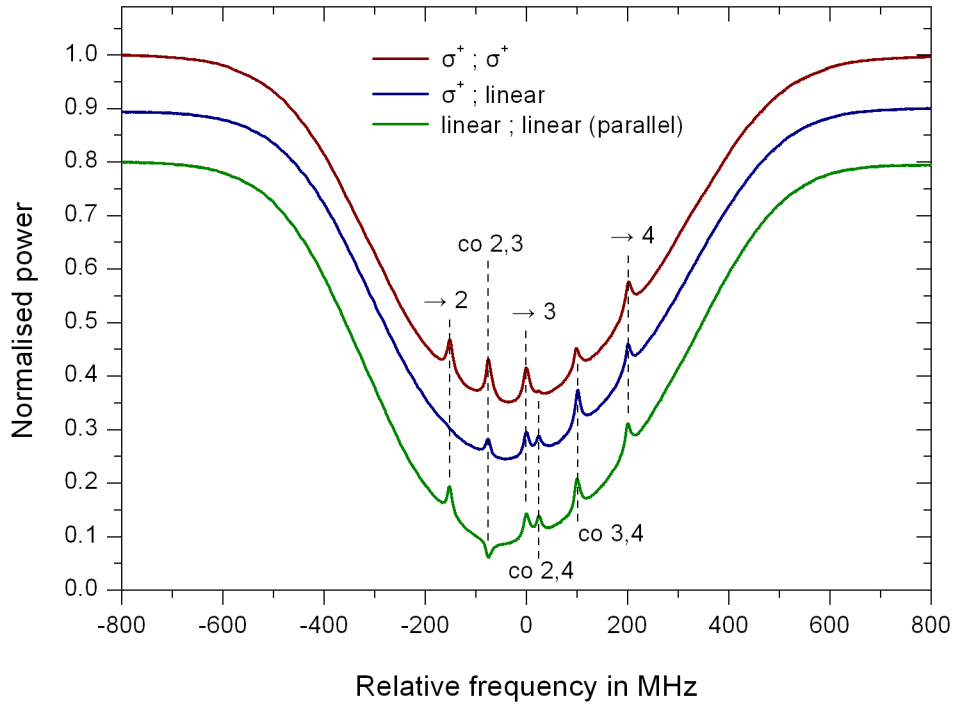

Figure 2.4: Saturated absorption spectra for different polarisations of the pump and the probe beam, $I_{pump}/I_{probe} \approx 4$, $T \approx 20\,°C$, from my reference spectroscopy setup. A ; B means an A polarised pump and a B polarised probe beam. The Lamb dips belonging to F' = 2, 3, 4 are indicated by → 2, 3, 4; co x,y stands for the crossover peak between F' = x and F' = y. The F = 3 → F' = 3 transition frequency is taken as zero. For a better visibility, the σ^- ; linear spectrum was vertically shifted by −0.1 and the linear ; linear spectrum by −0.2 .

For atoms with the mean velocity, optical pumping is expected not to occur using an OMF (see section 2.3). They only stay several nanoseconds in the light field and are at a maximum only excited once. But slow atoms which are long enough in the light field for several excitations get optically

pumped. Therefore, a change of the dip strengths and shapes with the change of the polarisations of the pump and the probe light might be observable. Taking the spectra from the caesium vapour cell (figure 2.4) as a reference, the dips in the spectra obtained with the OMF are a feedback for the polarisation of the pump and the probe light at the waist. With this spectroscopic method, it might be possible to determine the polarisation of the light at the waist of an OMF.

2.5 Polarisation spectroscopy

The optical pumping of the m_F levels induces an anisotropy of the caesium vapour resulting in a difference in the absorption coefficients for different polarisations of the light, $\Delta\alpha=\alpha^+-\alpha^-$, with $\alpha^\pm$ being the absorption coefficient for $\sigma^\pm$ - polarised light. A linearly polarised probe beam can be decomposed into two beams of equal amplitude, but with σ^+ and σ^- polarisations, that are absorbed to different degrees in an anisotropic medium. The probe beam, therefore, leaves the optically pumped caesium vapour with a rotated, elliptical polarisation. [20]

To measure the anisotropy, a saturated absorption spectroscopy setup with a σ^+ - polarised pump beam and a linearly polarised probe beam (spectrum in figure 2.4) is used.

After leaving the caesium vapour, the probe beam is split into two beams, with linear polarisations oriented orthogonally to each other using a polarising beam splitter (figure 2.5a). These are detected separately and the difference of their signals is calculated. The resulting polarisation spectrum is shown in figure 2.5b.

The signals in the polarisation spectrum are Doppler free, with the same arguments as for the saturated absorption spectroscopy, and occur at the transition and the crossover frequencies as well. The signals have a dispersive shape with the steep part at a transition or crossover frequencies. The large Doppler broadened linear absorption cancels nearly completely out.

For polarisation spectroscopy using OMFs, the transit time broadened parts of the spectra are expected to nearly cancel out as well, because they are dominated by fast atoms not optically pumped (see section 2.3 and 2.4). Therefore, the signals of the polarisation spectrum are dominated by slow atoms. For these slow atoms, effects due to the presence of the waist, like van der Waals shifts and surface induced anisotropy, can be studied [18].

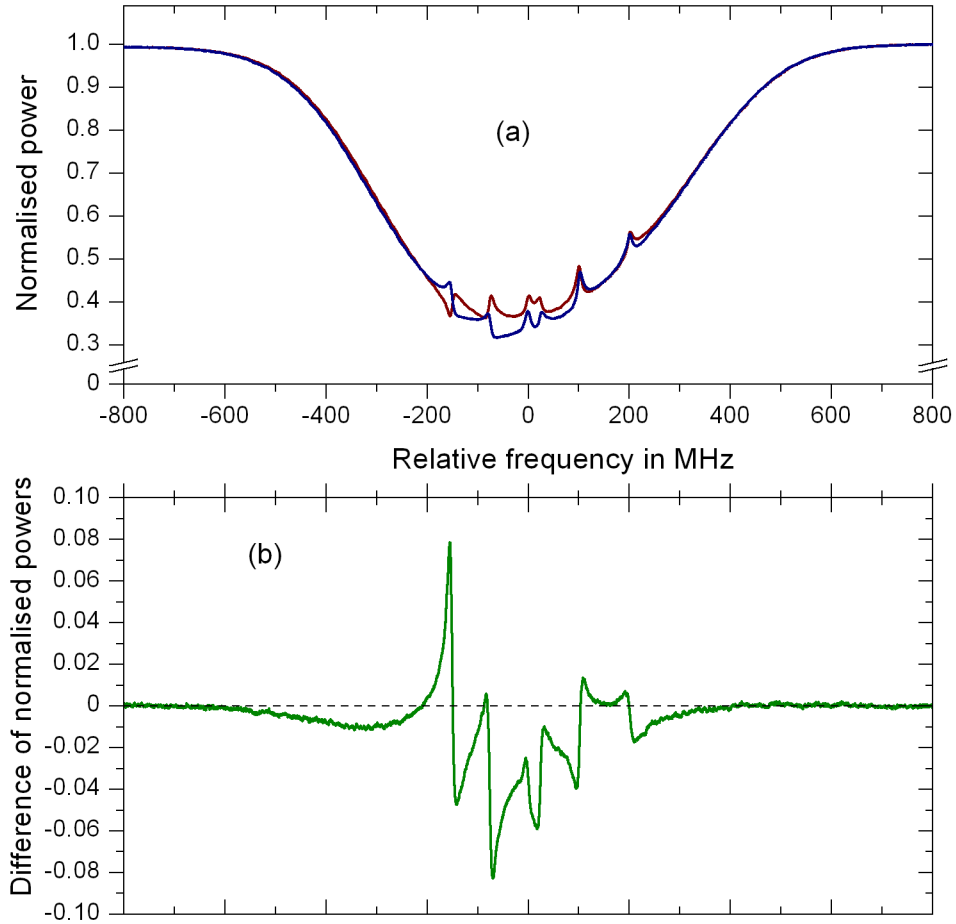Figure 2.5: Polarisation spectroscopy with σ^{+}- polarised pump and a linearly polarised probe beam, $I_{pump}/I_{probe} \approx 4$, $T \approx 20\,°C$, from my reference spectroscopy setup. The $F=3 \rightarrow F'=3$ transition frequency is taken as zero. (a) The decomposed probe beam after leaving the caesium vapour. (b) The resulting polarisation spectrum calculated as the difference of the components in (a).

3 Pump - probe spectroscopy of caesium vapour with OMFs

Using OMFs for pump - probe spectroscopy with the possibility of polarisation adjustment of the pump and the probe light and of measuring the anisotropy of the caesium vapour leads to several demands for the optical setup. In this chapter, I will describe these demands and the setup I built to fulfil them. The first results of my experiment and the appeared problems which were leading to the decision to protect the surface of our OMFs are presented in section 3.3.

3.1 Optical setup

Figure 3.1 shows a picture of the complete optical setup. The cover box for the laser is opened, the space inside was intentionally left free for a possible future addition of a second light source (see chapter 5).
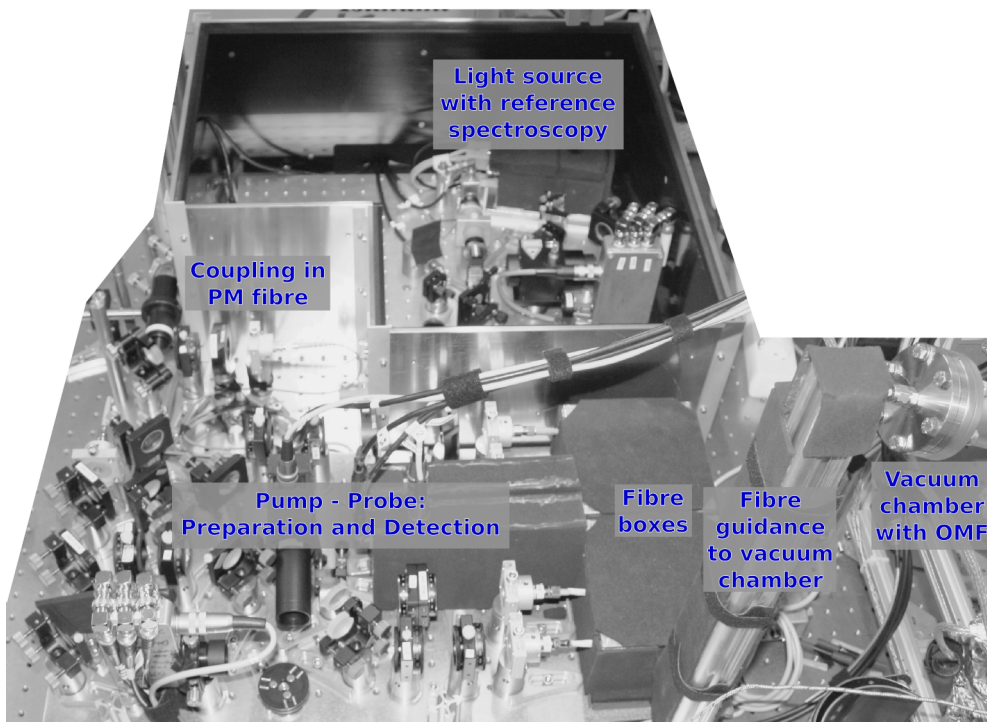
Figure 3.1: Picture of the complete optical setup with the opened laser box.

   The output beam from the light source with reference spectroscopy (see section 3.1.1) is coupled into a polarisation maintaining fibre and coupled out in the preparation and detection part for the pump and the probe beam (see section 3.1.2). The fibre ends of the OMF in vacuum chamber (see section 3.2) are guided down to the fibre boxes (see section 3.1.2) along an aluminium profile with thermal and vibrational isolation.

3.1.1 Light source with reference spectroscopy

Figure 3.2: Picture of the setup for the diode laser, the confocal Fabry-Perot cavity and the reference spectroscopy in the opened laser cover box.

As a light source for the frequency modulated caesium spectroscopy I built an extended cavity diode laser in Littrow configuration. The mechanical parts were made by our precision mechanical workshop, the original design i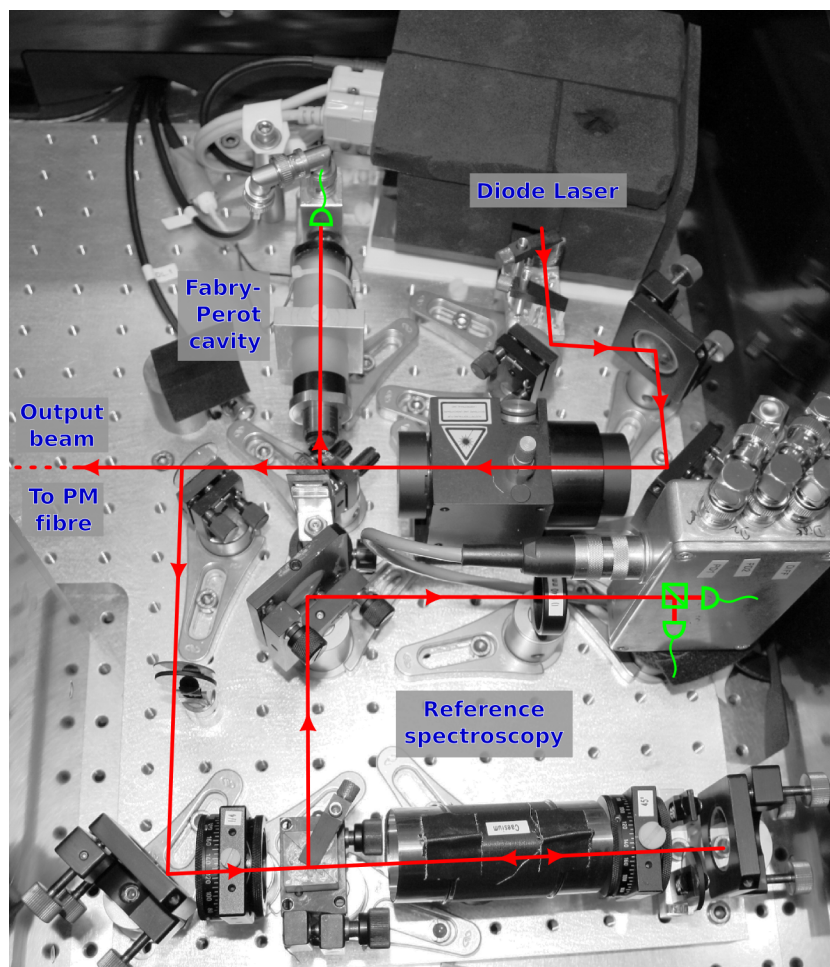s from [21]. The extended cavity given by a grating that delivers the feedback for the laser diode with its first order diffracted beam, while the zeroth order is used as the output beam.

By changing the angle between the grating and the beam of the laser diode with the help of a piezo actuator, the frequency of the light fed back into the laser diode is selected so that the diode laser can be scanned single mode and mode jump free over a range of about 6 GHz around the $F = 3 \rightarrow F' = 2, 3, 4$ transitions. The variation of the grating angle leads also to a displacement and a change of the direction of the output beam during scanning.

The current controller used for the diode laser is a Toptica DCC100/500mA, the scan controller for the piezo actuator a Toptica SC100.

Active temperature stabilisation is achieved using two Peltier elements, a temperature sensor and a Toptica DTC100/30W temperature controller. For vibrational and thermal isolation I glued foamed ethylene propylene diene monomer (EPDM) to the cover plates of the diode laser housing. But the high sensitivity of the diode laser to thermal and vibrational disturbances required additional isolation for the needed short and long time stability of the scanning laser. Therefore, I designed a cover box (figure 3.1) for the laser, the reference spectroscopy and the Fabry-Perot cavity (figure 3.2 and 3.3), which was built by our precision mechanical workshop. It has a sandwiched ceiling and sandwiched walls with, from outside to inside, 5 mm aluminium (10 mm for the ceiling), 5 mm foamed EPDM and 5 mm black polyoxymethylene (POM). Thereby, the desired stability of the laser was reached.

The light leaves the laser linearly polarised with the polarisation axis vertically oriented relative to the optical table. To compensate for the large horizontal divergence of the beam, a cylindrical lens telescope is used. The optical isolator is a tunable double stage 60 dB Faraday isolator (Linos DLI 1) adjusted to the 852 nm used (figure 3.3).

The Fabry-Perot cavity is used to verify that the diode laser is running single mode and mode jump free [15]. The mirrors of the confocal Fabry-Perot cavity have a radius of $R = 50 \, \text{mm}$ and a distance $d = 50 \, \text{mm}$, leading to a free spectral range $\Delta \nu_{FSR} = c / 4d = 1.5 \, \text{GHz}$ (c = velocity of light). To monitor also the frequency range between two transmission peaks, an oscillating voltage with about 0.5 Hz is applied to the piezo tube, on which one of the mirrors is glued.
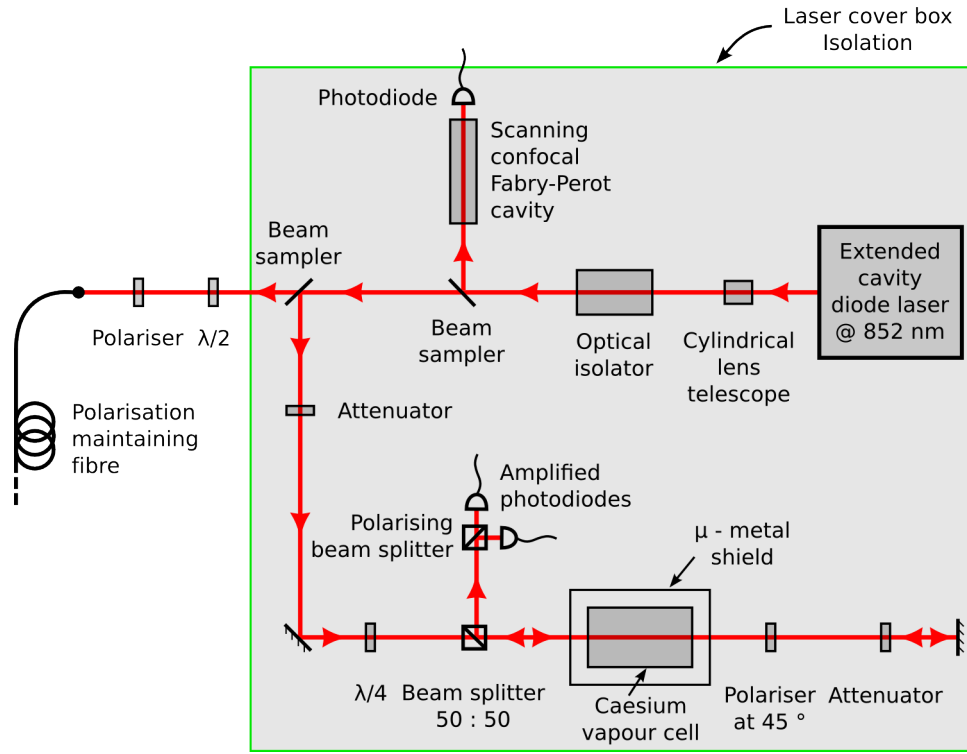
Figure 3.3: Schematic sketch of the setup for the light source and the reference spectroscopy.

For the reference spectroscopy I used the compact design from [22] for polarisation spectroscopy. In the standard adjustment, the linearly polarised light from the laser is changed with the quarter wave plate to σ^+ - polarised light and passed through the caesium vapour as the pump beam. The pump beam is then linearly polarised at 45 ° orientation with respect to the optical table using a polarise, back reflected and used as the counterpropagating probe beam. In the non-polarising beam splitter, 50 % of the light is separated from the pump beam, then decomposed in a polarising beam splitter and monitored with two amplified photodiodes. The sum of the signals of the photodiodes gives a saturated absorption spectrum (see section 2.3), the difference a polarisation spectrum (see section 2.5). Because the beam passes the caesium vapour twice, the Doppler broadened absorption background in the spectra is quite dominant. But pump and probe beam can be perfectly overlapped in this design, and I could not observe the

interferences mentioned in [22].

The light is coupled into a polarisation maintaining single mode fibre (Thorlabs P3-780PM-FC-2) after a short distance to reduce the effects of the beam displacement and change of the beam direction during scanning the laser with the grating. The coupling into the fibre can be adjusted in such a way that the light leaves the fibre with a nearly constant intensity over a scan range of about 2 GHz.

3.1.2 Pump - probe setup: Preparation and detection
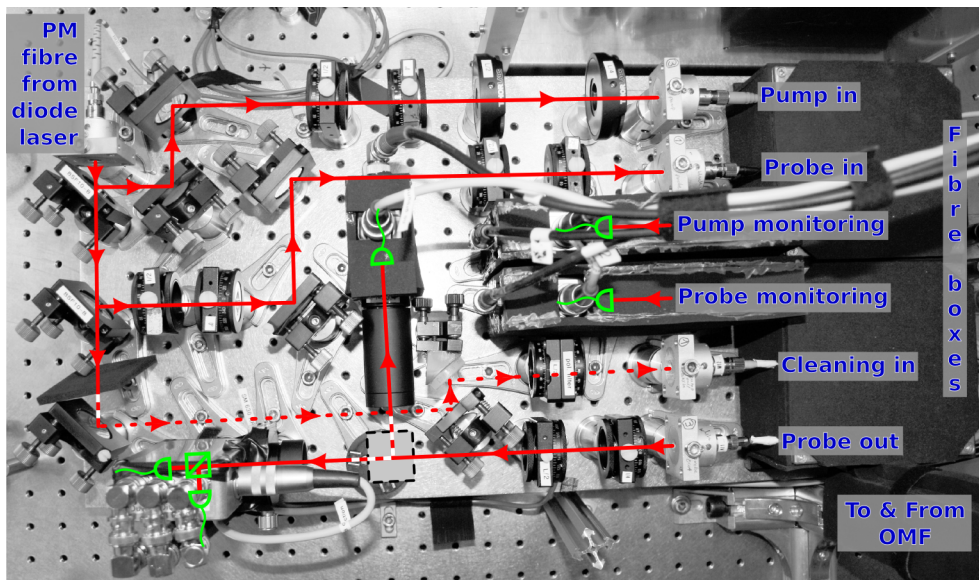
Figure 3.4: Picture of the setup for the preparation and detection of the pump, probe and cleaning light. The fibre system is in the isolated fibre boxes.

Light of the diode laser is guided to the pump and probe beam preparation and detection setup with a polarisation maintaining fibre (figure 3.5) and leaves it linearly polarised in vertical orientation with respect to the optical table (figure 3.5). About 1 % is split off with beam samplers for the pump and the probe beam.

With the attenuators consisting of a half wave plate and a polariser precise intensity adjustment of probe, pump and cleaning beam is possible.
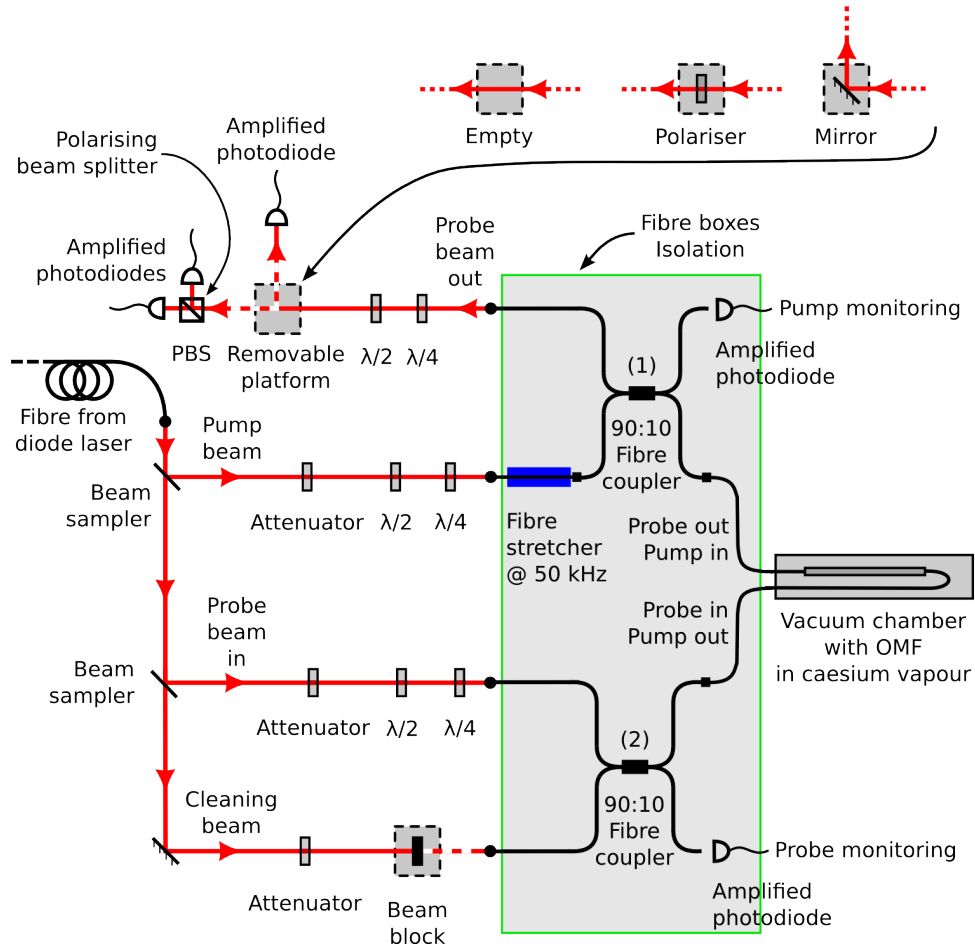
Figure 3.5: Schematic sketch of the setup for preparing the pump, probe and cleaning beams, the optical fibre system and the detection of the probe out beam.

Polarisation adjustment of the pump and the probe in beam

To study dependencies of the spectra on the polarisation of the pump and the probe light, it has to be possible to adjust their state of polarisation in the region in which they interact with the caesium vapour, which is the waist of the OMF. The whole fibre system connected to the OMF and the OMF itself consists of single mode fibres that are not polarisation maintaining. The

polarisation of light guided by a single mode fibre is in general not maintained due to the birefringences along the fibre. These birefringences can be intrinsic due to local imperfections of the fibre, for example small core deformations, or stress induced [23]. Mechanical stress factors leading to a birefringence in a fibre can be bending [24], twisting [25] and not radial symmetric squeezing [26]. Also, the temperature of a fibre influences its birefringences, a change in the temperature leads to a change of the birefringences [27]. The behaviour of the polarisation in the tapers of the OMF is not known and there might be birefringences in them as well.

For the following, only the birefringences of the fibre system were considered to influence the state of polarisation of the light guided. The overall effect of arbitrary combinations of birefringences can be described as the effect of a single birefringence [28]. Therefore, for all the stress and intrinsic factors influencing the birefringences of a fibre being constant over time, the effect on the state of polarisation of light guided over a certain fibre length can be summed up as the effect of a single and constant birefringence. By adjusting the state of polarisation of the pump and the probe beam before the coupling into a fibre, it is possible to achieve the wanted state of polarisation at the waist of the OMF [28].

One can conclude this by taking two subsequent changes of the polarisation of the incoming beam which can be combined in a single one. The polarisation of the beam is first changed to the wanted polarisation at the waist. Then it has to be changed to compensate for the effect of the birefringence of the fibre system.

With a half wave plate and a quarter wave plate it is possible to change the linearly polarised pump and probe beam to an arbitrary state of polarisation (see figure 3.5) and, therefore, to achieve the wanted state of polarisation of the light at the waist of the OMF. A feedback of the actual state of polarisation of the light at the waist might be given by the shape of the saturated absorption and polarisation spectrum, see section 2.4 and 2.5.

Isolation of the fibre system

To achieve stable birefringences (see above), the whole fibre system has to be kept mechanically stable and thermally and vibrationally isolated. To achieve the needed isolation, I put the fibres into aluminium boxes and covered the fibre system with EPDM. A verification of the stability of the birefringences of the fibre system due to this isolation is given by the stability of the observed interferences due to backreflections (figure 3.6), as

they depend also on the polarisation of the interfering beams. With the aluminium boxes for the fibres opened, vibrations and temperature fluctuations lead to fast and random changes of the position and the shape of the interference signal. In contrast, closing the boxes and letting the fibre system relax and thermalise for about a day give an interference signal, which has a constant shape and is not moving at all.

Intensity monitoring of the pump and probe in light

The $90:10$ single mode fibre couplers (Thorlabs FC850-40-10-APC) in figure 3.5 allow monitoring of the intensity of the light actually coupled into the fibre system. Free space beam splitters [17] only allow monitoring of the intensity of the light before it is coupled into a fibre. By using the fibre couplers, a decoupling of the monitored intensity form the coupling losses is achieved. 90 % of the pump and the probe beam coupled into the fibres are sent to the amplified photodiodes, 10 % to the OMF, which allows precise adjustment and monitoring of low intensities of pump and probe light at the waist of the OMF. For the probe light leaving the OMF, 90 % reach the detection part.

  The signal of the amplified photodiodes for intensity monitoring is first calibrated to the power of the light leaving the fibre couplers without an OMF connected. Connecting one fibre end of the OMF to the probe in arm of the fibre coupler (2) and measuring the power transmitted at the other end gives the transmission through the OMF. This is initially done with an OMF in the vacuum chamber before it is exposed to the caesium vapour. The other fibre end of the OMF is then connected to the probe out arm of fibre coupler (1). The sum of the signals of the amplified photodiodes in the probe out beam detection part is calibrated to the known power leaving the OMF, and thus to the transmission of the OMF. As a result, the absolute intensity of the pump and the probe light reaching the OMF and the transmission through the OMF can be monitored during the experiment.

  For optimisation, the used fibre connecting technique needs to provide reproducible transmissions through the fibre connections, because one can not distinguish between a loss of the light in a fibre connection or within the OMF. Gel splices (3M 2529 universal splices) turned out to fulfil this criterion. A measurement of the transmission of six splices of single mode fibres (Fibercore SM800) gave an average transmission of 98.9 % at 852 nm, with the lowest transmission being 97.5 %. Therefore, I used these splices to connect the OMF and the fibre stretcher (see below) to the fibre

couplers.

Detection of the probe out light

By leaving the removable platform (figure 3.5) empty, the probe out beam is split with a polarising beam splitter into two linearly polarised beams with their orientation of the polarisation orthogonal to each other. The beams are monitored separately with amplified photodiodes, their sum gives a saturated absorption spectrum, their difference a polarisation spectrum. Due to birefringences in the fibre system between the OMF and the out coupling, the polarisation of the probe out beam has to be adjusted to measure the anisotropy. This is done at a frequency at which no anisotropy is expected, for example at the left and right ends of the Doppler broadened absorption dip. With the quarter wave plate the light is first changed to be linearly polarised. The orientation of the linear polarisation is then rotated with the half wave plate to give equal signals of the photodiodes. This adjustment is done with the help of a polariser, which is mounted on a removable platform and can be added if needed.

  For very low intensities of the probe out beam, a single amplified photodiode can be used to obtain a better signal to noise ratio by adding a mirror mounted on a removable platform (figure 3.5).

Cleaning beam

The cleaning beam sketched in figure 3.5 can be used for cleaning the waist and the tapers of the OMF with light [1][29]. By removing the beam block for a moment, light with powers up to a few hundred microwatts is sent to the tapers and the waist of the OMF, leading to a partial removal of caesium atoms adsorbed to the surface due to heating effects and light induced atomic desorption [30].

Interferences

A problem with counterpropagating light in optical fibres is the occurrence of interferences due to backreflections at the end facets of the fibres. In contrast to free space beam setups, in which a slight tilting of the optical elements leads to separation of, for example, the backreflection of the pump

beam from the probe beam, one can not avoid this problem using optical fibres. Even at the FC/APC end facets with an angle of 8 ° relative to the fibre axis, a small amount of the light leaving the fibre is reflected under such an angle that it is guided back by the fibre. The intensity of two interfering waves with the same polarisation is given by

$$I = I_1 + I_2 + 2 \cdot \cos(\Delta \Phi) \cdot \sqrt{(I_1 \cdot I_2)} \ ,$$

with $I_{1,2}$ the intensities of the two waves and $\Delta \Phi$ their phase difference at the location of the interference. To obtain a peak to peak amplitude of the interference signal of 4 % as in figure 3.6 with counterpropagating probe and pump light, $I_{pump}/I_{probe} \approx 4$, an intensity of the backreflected pump light of only $I_{br,pump} = I_{pump} \cdot 2.5 \cdot 10^{-5}$ and identical polarisations of the probe light and the backreflected pump light at the location of the interference are needed:

$$\Delta I_{interference} = 4 \cdot \sqrt{I_{probe} \cdot 4 \cdot 2.5 \cdot 10^{-5} \cdot I_{probe}} = 0.04 \cdot I_{probe} \ .$$

Due to several end facets along the way of the pump light in the fibre system, several backreflections and the probe light can interfere, determined by their polarisations and thus by the adjustment of the polarisations of the pump and the probe beam coupled into the fibre system (figure 3.6).

Not sketched in figure 3.5 are cut single-mode patch fibres (Thorlabs P3-830A-FC-2) between the fibre couplers and the OMF. The bare fibre end is spliced to the OMF using 3M 2529 gel splices, the FC/APC terminated end of them is permanently connected to the fibre coupler with mating sleeves (Thorlabs ADAFC2-PMN). Although index matching gel (Thorlabs G608N) was used, these FC/APC end facets give backreflections contributing to the interferences as well.

Furthermore, at the tapers and the waist of the OMF light can be backreflected or backscattered and coupled back into the fibre.

With the frequency of the laser being scanned, the distance of the interference peaks in a spectrum, $\Delta\nu_{FSR}$, is determined by the difference of the optical path lengths of the probe and the backreflected light, ΔL , by $\Delta\nu_{FSR} = c/(n \cdot \Delta L)$, with c = velocity of light and n = refractive index of the medium. The path length differences of the free space beams can be neglected compared to fibre lengths of several metres. Taking the lengths of the fibres to be 1 m to 10 m for the different backreflections and the refractive index of the optical fibres to be about 1.45, $\Delta\nu_{FSR}$ goes from

about 20 MHz to about 200 MHz, thus being in the same region as the distances of the Lamb dips and crossover peaks (figure 3.6).
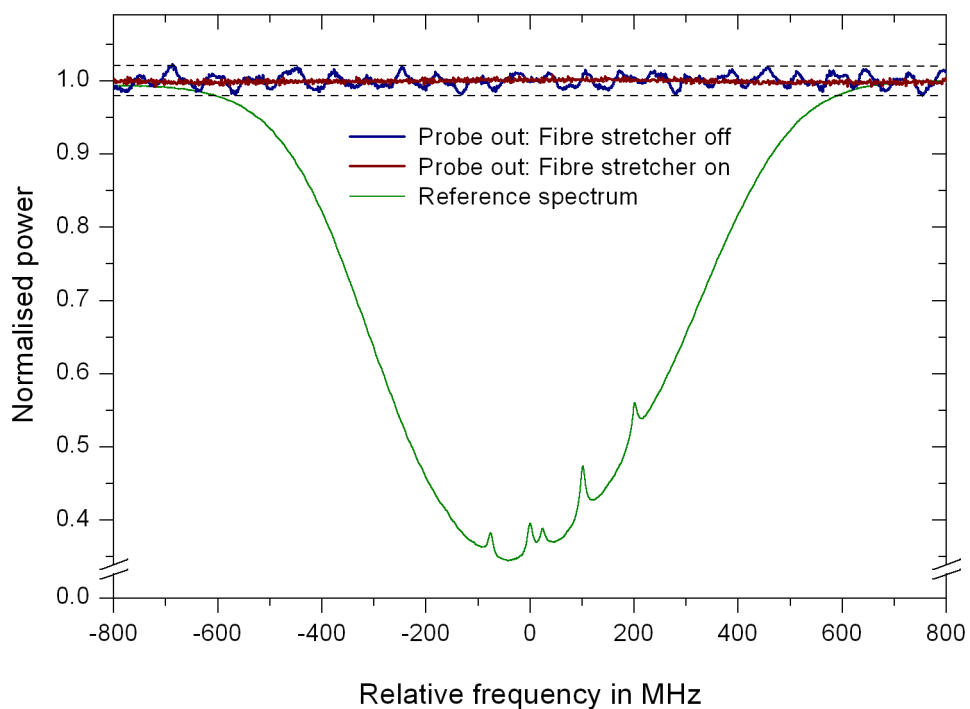

Figure 3.6: Example for the effect of the fibre stretcher at about 50 kHz on the interferences of the fibre system, the dashed lines are at $1 \pm 2\%$. Probe out signals: Instead with an OMF (figure 3.5), the fibre couplers were directly connected with a 3M 2529 gel splice. The polarisations of the pump and the probe beam were adjusted to give a dominant frequency component in the interference signal. $I_{pump}/I_{probe} \approx 4$; signals normalised to the probe out signal with the fibre stretcher switched on; frequency calibration due to a reference spectrum, the $F=3 \rightarrow F'=3$ transition frequency is taken as zero. Reference spectrum: σ^+ - polarised pump and linearly polarised probe beam, $I_{pump}/I_{probe} \approx 4$.

Fibre stretcher

To get rid of the interferences in the spectra, I built a fibre stretcher (figure 3.7).
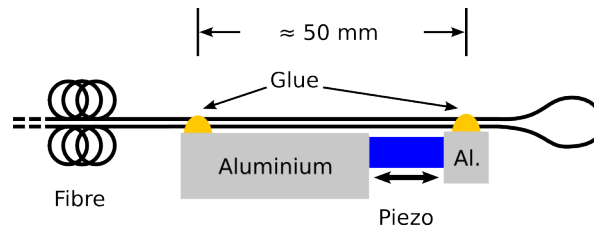

Figure 3.7: Sketch of the fibre stretcher.

The purpose of this device is to induce a fast oscillating change of the optical path length with a peak to peak amplitude of $\Delta d > \lambda / 2 = 426 \, \text{nm}$, of the pump beam before it is split in the fibre coupler (figure 3.5). This transfers the interference signals to such high frequencies that they can be filtered out by a low pass filter without disturbing the signals from the spectrum.

The design of the fibre stretcher is sketched in figure 3.7. A low voltage piezo actuator is glued to a larger aluminium block and a small aluminium block is glued to the piezo actuator. The coating of the fibre is removed over a length of a few millimetres where the fibre is to be glued and then fixed to the aluminium blocks with the help of a two component epoxy adhesive. By applying a voltage to the piezo actuators, the piece of fibre between the glue points is mechanically stretched or squeezed and the optical path length is changed. I have chosen the rather large distance between the glue points of about 50 mm to reduce the relative stretching of the fibre and thus the risk of damaging it. By using the fibre arrangement in figure 3.7, the absolute length change is doubled and mechanical stress on the fibre ends leading to changes of the birefringence during stretching is reduced.

In order to let the stretcher oscillate with the desired high frequency, it has to be driven at its resonance frequency. The high frequency limit is given by the excitation of standing compression waves in the fibre. For the first excitable longitudinal compression wave with a half wavelength $\lambda / 2 \approx 50 \, \text{mm}$ and the speed of sound in fused silica $c_{s, fs} \approx 6 \cdot 10^3 \, \text{m/s}$, the frequency is given by $\nu_{\lambda / 2 \approx 50 \, \text{mm}} = c_{s, fs} / \lambda \approx 60 \, \text{kHz}$. The highest resonant frequency showing an effect on the interferences was found at about

50 kHz. With this stretching frequency and a scanning frequency of the laser of about 30 Hz, the interferences can be filtered out to a high degree using the HiRes mode of the oscilloscope (Tektronix DPO4104) and 1000 acquisition points (figure 3.6). Taking the scan range of the laser to be about 2 GHz, one gets the distance of the frequencies of two interference maxima in the spectrum to be $\Delta \nu_{FSR} \approx 2 \cdot 30\,\text{Hz} \cdot 2\,\text{GHz}/50\,\text{kHz} = 2.4\,\text{MHz}$. One could achieve the same result by increasing the length of the fibre in which the pump beam is coupled before the fibre coupler (figure 3.5) by $\Delta L \approx c/(n \cdot \Delta \nu_{FSR}) \approx 86\,\text{m}$ (see the interference section above), with the advantage of being independent of the scanning frequency of the laser.

3.2 Vacuum chamber

The vacuum chamber and its heating system are described in detail in [1], so I will give only a short description of the applied standard procedure here. A schematic sketch of the vacuum chamber is shown in figure 3.8.
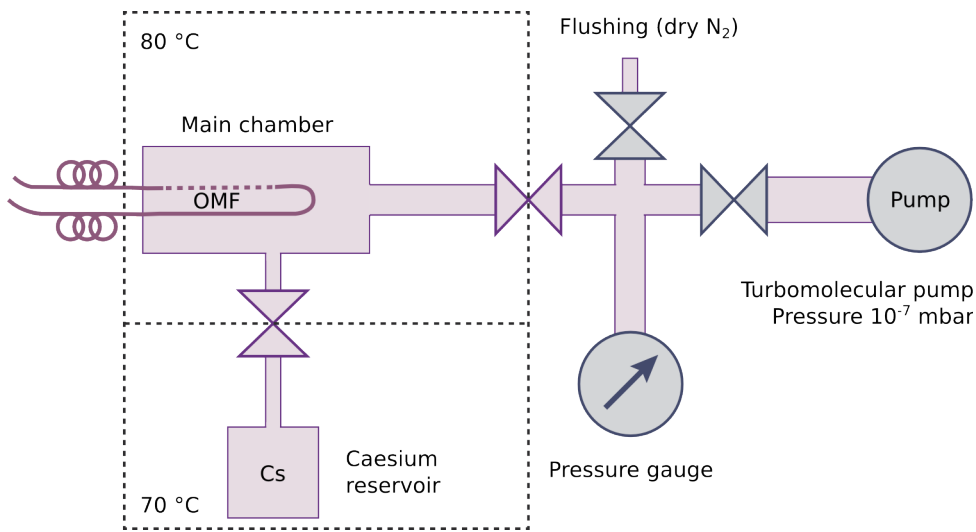

Figure 3.8: Schematic sketch of the vacuum chamber system with an OMF. *Reproduced from [1]*

Before mounting an OMF in the main chamber, the valves to the pump and the caesium reservoir are closed. The opened main chamber is flushed

with dry nitrogen to avoid water from the ambient air entering the chamber. The OMF in its holder, with the cover removed (figure 1.3), is clamped to the walls of the main chamber and the main chamber is closed. The fibre ends of the OMF are fed through chamber wall using a specially designed Polytetrafluoroethylene (PTFE) ferrule feedthrough. After closing the valve to the nitrogen and opening the valve to the pump, the chamber is pumped out. During pumping out, the main chamber is heated to 80 °C and the caesium reservoir to 70 °C. The temperature of the main chamber is chosen because of the temperature limitations of the acrylic coating at the fibre ends of the OMF (figure 1.3). To prevent the caesium from condensing in the main chamber, the temperature of the caesium reservoir is kept well below the temperature of the main chamber.

Up to this point, the transmission of the OMF is monitored continuously using a white light source (Ocean Optics LS-1) and a silicon power meter (Thorlabs S120VC head at Thorlabs PM100USB, logged with a computer). After reaching a stable pressure of a few 10^{-7} mbar within a few days, the OMF is connected to the fibre system and the signals of the photodiodes are calibrated (section 3.2).

Then the valve of the main chamber to the pump is closed and the valve to the caesium reservoir is opened, so that a hot atomic caesium vapour can build up around the OMF.

3.3 First results

With an OMF being exposed to the hot caesium, a linear absorption within the first day could be observed (figure 3.9).

The measured dip depths of about 5 % with a few nanowatts probe power are in agreement with [1]. During the first day in caesium vapour the transmission of the OMFs decreased by at least 50 % and went unrecoverably down to zero within two days. After removing the OMFs from the chamber, ripped waists could be observed. This behaviour was the same for the three OMFs used for subsequent experiments.

Attempts to recover the transmissions by cleaning with light were only partially successful. The transmissions could be increased by up to 100 %, but started decreasing quickly afterwards. When the transmissions went down to zero or almost zero, cleaning with light did not show an effect any more.
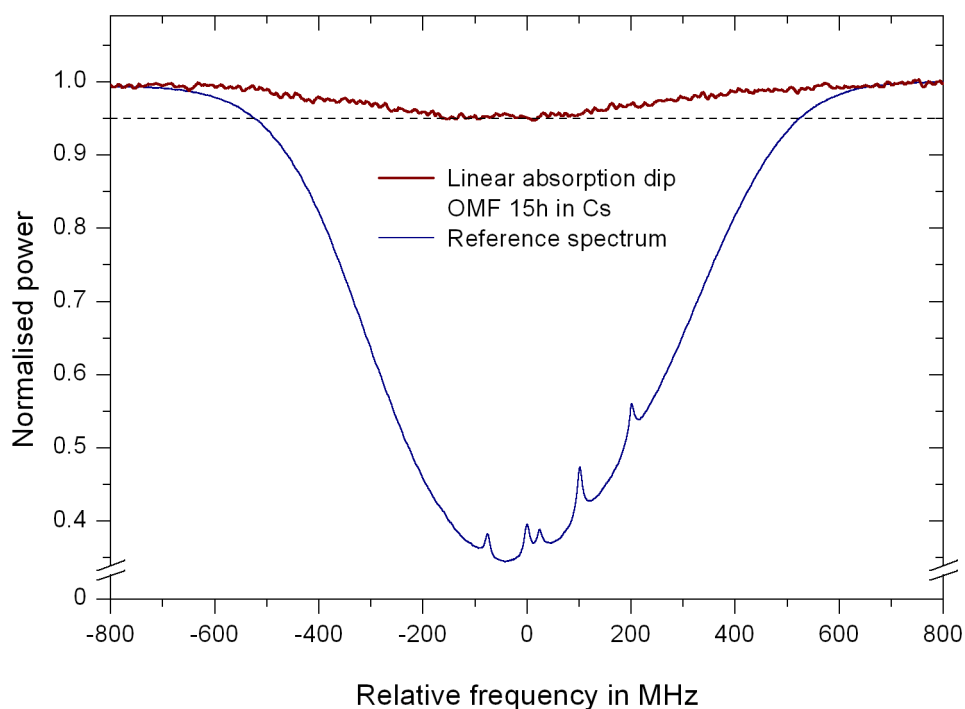
Figure 3.9: Example for the linear absorption dip measured with an OMF within the first day in caesium vapour. Probe power reaching the OMF $P_{probe} = 10\,nW$; transmission of the OMF before exposed to caesium vapour $T_0 = 66\%$; transmission of the OMF after exposition to caesium vapour for 15 h $T_{Cs,15h} = 34\%$; frequency calibration due to a reference spectrum, the $F = 3 \rightarrow F' = 3$ transition frequency is taken as zero. Reference spectrum: σ^+ - polarised pump and linearly polarised probe beam, $I_{pump} / I_{probe} \approx 4$.

During the time the OMFs transmitted light, no effect of the pump light could be observed. The caesium needs several days to build up a sufficient vapour density in the chamber [1] so that the absorption by the caesium atoms gets strong enough to resolve the saturated absorption signals.

As a reason for the loss of the transmission of the OMFs the vacuum chamber system without caesium vapour could be excluded. An OMF in the vacuum chamber showed a stable transmission during heating and pumping out for two weeks. With the valve of the main chamber to the pump and the caesium reservoir closed (figure 3.8), the transmission of this OMF stayed

stable for a week, until the caesium reservoir was opened.

To exclude that pollutions at the inner walls of the chamber react with the caesium and produce substances that evaporate and adsorb to the surface of the OMF, which leads to the transmission loss, the main chamber was mechanically cleaned and the vacuum chamber was baked out at about 200 °C for several days. This cleaning showed no observable effect on the transmission loss of an OMF used for the experiment afterwards.

Due to the measurements presented in [1], it can be excluded that in general the exposure of an OMF to a hot atomic caesium vapour causes a transmission drop of the OMF to zero within two days.

The most probable reason for the transmission loss of the OMFs is, therefore, that chemical reactions of the caesium atoms with molecules adsorbed at the surface of the OMFs or with the silanol groups (see 1.3) lead to a destruction of the waist of the OMFs.

Although the exact reasons for the transmission loss of the OMFs are not known, we concluded that chemical reactions at the surface of the OMFs with the caesium were leading to the destruction of the OMFs. To overcome this problem, we decided to try to find a way to protect the surface of our OMFs against this. To make the OMF withstand a hot atomic caesium vapour, I have chosen to chemically passivate the surface of an OMF.

4 Chemical passivation of the surface of an optical microfibre

Due to the high sensitivity of OMFs to damages caused by mechanical and chemical influences, different protection and passivation techniques were developed, see, for example, [31]. But these techniques are not suitable for OMFs exposed to atomic caesium vapour. In this chapter I will give a short introduction to a chemical passivation technique with which OMFs for caesium spectroscopy can be protected and present the developed treatment procedure of an OMF.

4.1 Initial situation

The surface of our OMFs is expected to have the same chemical properties as the surface of fused silica, see section 1.3. Therefore, we expect surface adsorbed molecules and the silanol groups to react with the caesium.

The average density of the silanol groups is taken to be about one per square nanometre and approximately constant (see section 1.3). But the amount and kind of the adsorbed molecules depends on the environmental conditions and the time an OMF was exposed to these.

Before the pulling process of an OMF (see section 1.2), the acrylic coating of the optical fibre is removed and the fused silica surface is thoroughly wiped with organic solvent wetted lens tissues. During the pulling process, the oxygen-hydrogen burner heats the surface of the fibre to at least 1500 °C [6], so that surface adsorbed molecules are expected to be removed afterwards. Thus, we expect our OMFs to have an initial clean fused silica surface with siloxane and bare silanol groups (figure 1.4). After the pulling process, the OMFs are fixed to a aluminium holder, protected against mechanical stress and dust and stored under ambient conditions. During this time, various molecules can adsorb to the OMF surface.

Water molecules form molecular layers at a silica surface, with their number depending on the humidity of the environment [7][8]. The water molecules build hydrogen bridges to the silanol groups and other water molecules, leading to strongly bound layers. For removing the first water layer on the surface, temperatures well above 100 °C are required [13][32][33], which exceed our limitations significantly (see section 3.2).

Other molecules from the air can bind to the adsorbed water molecules or get solved in the surface water. They can also bind directly to the silanol

groups chemically or via hydrogen bridges. Due to the low electronegativity of silicium compared to oxygen, the siloxane and silanol groups at the silica surface lead to a negative surface charge, so that the electrostatic binding of molecules and dust can be quite strong.

Some of the surface adsorbed molecules can be removed by rinsing the OMF with solvents and during heating and pumping out (see section 3.2). But due to the limitations given by our OMFs, only a partial removal is possible. Therefore, the chemically very reactive caesium atoms react with the silanol groups, the surface water and the various surface adsorbed molecules on the OMF. The silica can be damaged due to reactions with the reaction products or with the caesium atoms themselves. Because of waist diameters of about 0.4 μm , small damages, like cracks or pores, can lead to a rip of the waist. With the high intensity of the light at the surface, the transmission of an OMF is very sensitive to light absorbing molecules and atoms at the surface and to structures at the surface which scatter the light. Thus, the transmission of an OMF can be lost due to the reaction products absorbing the light, etching structures in the silica or forming structures at the surface, also in combination with the caesium atoms, which scatter the light.

Depending on the actual type and amount of the surface adsorbed molecules and, thus, on the history of an OMF, these effects can occur with different strengths and on different time scales. For adsorbed molecules not reacting with caesium, also a protective coating effect is possible.

4.2 Approach

To avoid transmission losses of the OMF due to chemical reactions with the caesium atoms and thus obtain reliable and reproducible times for which an OMF can be used for spectroscopy in a hot atomic caesium vapour, we decided to passivate the surface of an OMF. In detail, this passivation should prevent chemical binding of molecules to the surface, make the surface hydrophobic to reduce the amount of adsorbed water and give a surface with a low binding energy to reduce physical adsorption of molecules and caesium atoms. Such a passivation is achieved by a treatment which gives a surface of the OMF out of molecular end groups with the desired properties.

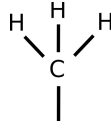We decided to try to get methyl groups (-CH$_3$) as end groups on the surface of our OMFs, figure 4.1.

Figure 4.1: Methyl group, -CH$_3$

Although their exact properties depend on the rest of the molecule, methyl groups are in general chemically inert up to a few hundred degree Celsius, hydrophobic and have a low binding energy. Various molecules with methyl groups as end groups have been used for wall coatings of caesium vapour cells and glass cells in vacuum systems with caesium vapour, see, for example, [34][35][36][37], proofing the chemical long time stability of methyl groups exposed to atomic caesium and their low surface binding energy. The electrostatic surface potential of the methyl groups is positive, so that electrostatic binding of dust, molecules and atoms is still possible.

But we have several other additional demands for the treated surface of an OMF and the procedure of the treatment:

- We want a vacuum stability of the treatment effect down to 10^{-7} mbar (see section 3.2).

- The temperature stability of the treatment effect has to be given up to a few hundred degree Celsius. Although we only heat the OMF up to about 80 °C (see section 3.2), local heating of the waist due to absorption of the light by, for example, surface adsorbed caesium atoms can lead to such high local temperatures.

- To preserve the optical properties of our OMFs (see section 1.1), the maximum height of the applied structures on the surface has to be a few nanometres. A uniform coating with a constant thickness increases the diameters of the waist and the tapers, leading to a change of the optical properties of an OMF. Local structures at the surface scatter the light and lead to a low transmission of the OMF.

- The molecules at the surface after the treatment have to be transparent for light with the used wavelength, 852 nm. At the waist of an OMF, the light is guided along the surface over several millimetres with high intensities at the surface (see section 1.1), so

that already a small absorption of the single, surface adsorbed molecule leads to a significant transmission loss of the OMF [6].

- The procedure for passivating the surface of an OMF is limited by the high sensitivity of the OMF to mechanical, vibrational and temperature induced stress. The maximum temperature during the whole treatment procedure has to be kept at about 80 °C, mechanical and vibrational stress has to be avoided. The stress induced by rapid temperature changes can lead to a damage of the OMF as well.

A commonly used method for wall coatings of caesium vapour cells is to bring a film out of alkanes, C_nH_{2n+2}, or polydimethylsiloxanes (PDMS), $(H_3C)_3SiO[Si(CH_3)_2O]_nSi(CH_3)_3$, to the cell walls. Although alkanes have mainly $-CH_2$ end groups, I mention them here due to their frequent usage and similar properties. Film coatings with alkanes or PDMS are not suitable for treating an OMF. The coating effect of alkane and PDMS films is not stable up to the desired temperatures and their vacuum suitability is not given down to pressures we want to achieve, because they loose the viscosity needed to form a film and start heavy outgassing below about 80 °C.

Another approach is to get molecules chemically bound to the silanol groups at the silica surface. These molecules need a head group which allows the chemical binding to the silanols and a tail group which determines the actual surface properties. We want a passivated surface, so molecules with methyl groups as tail groups are chosen.

For a stable chemical binding of the molecule to the silica surface, a siloxane group ($\equiv$Si-O-Si$\equiv$) is a good choice for the resulting bound head group. Therefore, a silyl head group consisting of a silicium atom and at least one chemical reactive end ($R^{reactive}$) is needed, $-Si-R^{reactive}R^2R^3$, with R^2, R^3 other ends. Due to our limitations in the treatment temperatures, I have chosen chlorine as the reactive end, as it is the most reactive one [7].

The further specification of the molecules to use requires considering additional limitations. For the time this work was done, no technique was available to characterise the treated surface of an OMF in detail. A commonly used technique for analysing a silica surface is infrared spectroscopy to obtain information about the vibrational spectra of the adsorbed molecules [38][39]. From these spectra it can, for example, be deduced what molecules adsorbed to the surface and whether the wanted chemical binding took place. The wavelengths needed are above 1500 nm [39][38] and are not transmitted by OMFs used for 852 nm, as well as light

in the ultraviolet range, which is needed for analysing the electronic transitions of the adsorbed molecules.

Therefore, the feedback needed to adjust the treatment parameters was not available. Thus, I was limited to the use of molecules with treatment procedures which are well described in the literature and not sensitive to small variations of their parameters. Concerning the transfer of procedures from the literature to our OMFs, the used silica type has to be considered. Many different types of silica are used, differing, for example, in their micro- and nanostructure of the surface, their average (hydroxylated) silanol group density, and the arrangement of the (hydroxylated) silanol groups (see figure 1.4) [13][7].

As a consequence, attempts for getting a self assembled monolayer (SAM) of long silanes, like octadecyltrichlorosilane (OTS) with methyl groups as tail groups, $CH_3(CH_2)_{17}SiCl_3$, were not made. The success of a treatment, which means the growth of a monolayer, is very sensitive to residual water in the used solvents [32]. Additionally, no statement can be made whether the actual chemical binding of an OTS SAM to the surface of fused silica leads to our desired vacuum and temperature stability.

I have chosen to try to silylate the surface of an OMF with small methylchlorosilanes (figure 4.2).
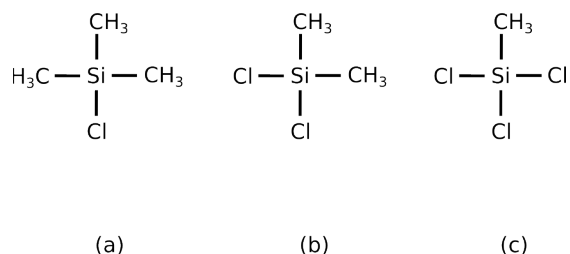

Figure 4.2: The smallest methylchlorosilanes: (a) Trimethylchlorosilane (TMCS), $(H_3C)_3SiCl$, (b) Dimethyldichlorosilane (DMDCS), $(H_3C)_2SiCl_2$, and (c) Methyltrichlorosilane (MTCS), $(H_3C)SiCl_3$

4.3 Silylation of a fused silica surface with methylchlorosilanes

4.3.1 Chemical reactions

Silylation of glass surfaces with methylchlorosilanes is a commonly used treatment to obtain passivated surfaces, see, for example, [40]. The reaction scheme for one of the standard procedures [39] is shown in figure 4.3. The silica is baked out and exposed to a methylchlorosilane vapour, both at few hundred degrees. Due to the baking out, the water layers are removed from the silanol groups (dehydrated) and the silane reacts with the hydroxyl group (-OH) of the silanol. The hydrogen of the hydroxyl group forms with a chlorine from the silane hydrogen chloride, HCl, so that the methylsilyl group, $-Si(CH_3)_3$ for TMCS, binds chemically to the oxygen of the silanol, forming a trimethylsiloxane, $\equiv Si-O-Si(CH_3)_3$, end group. The silicium atoms are strongly bound due the $\equiv Si-O-Si\equiv$ siloxane group. The methyl groups, in case of the TMCS three of them, arrange above the former silanol group and cover a certain surface area, see figure 4.3.
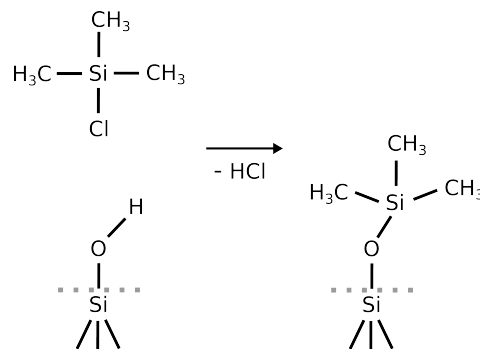

Figure 4.3: Silylation of an isolated silanol group with TMCS in vapour. The silica surface is dehydrated, temperatures of a few hundred degree Celsius are needed. *Reproduced from* [39]

The silanol group is now chemically deactivated and the methyl groups cover a certain surface area. This area has a low binding energy and is hydrophobic. The chemical binding of the methyl groups gives the desired vacuum and temperature stability [34][39].

The high temperatures needed can be avoided by exposing a hydrated silica surface to a, for example, trimethylchlorosilane vapour, the reaction
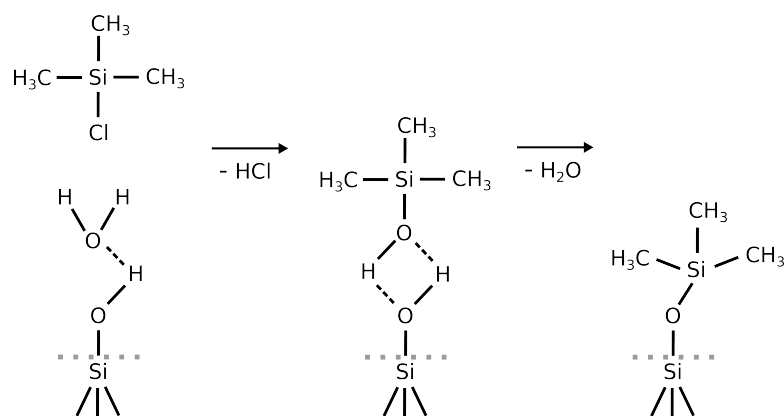
scheme [41][42] is shown in figure 4.4.

Figure 4.4: Silylation of an isolated silanol group with TMCS in vapour. The silica surface is hydrated, ambient temperatures are enough. *Reproduced from* [41]

A hydrated silica, indicated by the water molecule bound to the hydroxyl group via a hydrogen bridge in figure 4.4, is exposed to a TMCS vapour. In a first step, the TMCS is hydroxylated by the surface water with the release of HCl. The hydroxyl groups of the trimethylsilanol and the surface silanol form hydrogen bridges, leading to a already strongly bound trimethylsilanol layer on the silica surface. In a second step, the trimethylsilanol condenses down to the surface with the release of water, ending in the same situation as in figure 4.3.

Only ambient temperatures during the whole procedure are needed to obtain a complete condensation at the silanol groups within a few minutes using TMCS and DMDCS [42]. For MTCS to condense fully down at ambient temperatures, a pretreatment of the silica surface with a promoter, for example triethylamine (TEA) in vapour, has be done [43].

The three methylchlorosilanes (figure 4.2) differ in their number of reactive ends and thus in the number of surface silanol groups or other methylchlorosilanes they can bind to [43].

TMCS has only one reactive end and thus only binds to one silanol group. For a TMCS binding to a silanol group with another one near by, see figure 1.4c-d, it can prevent a second TMCS from binding to this silanol group by occupying the space needed. Therefore, there is the risk that some silanol

groups are not deactivated.

DMDCS has two reactive ends and can bind to two silanol groups close together. MTCS has three reactive ends, but can only bind to two silanol groups as well due the molecular angles and distances.

Methylchlorosilanes can also bind to other methylchlorosilanes at ambient temperatures under certain circumstances. As a first point, they need to be hydroxylated, see figure 4.4. For this hydroxylation water has to be available in the vapour, the solution or at the solid-gas interface.

TMCS has only one reactive end and can, therefore, only form hexamethyldisiloxane (HMDS), $O[Si(CH_3)_3]_2$. The methyl groups of the chemically surface adsorbed TMCS only cover the surface areas around the silanol groups, so that some areas with surface siloxane groups are left out.

DMDCS with its two reactive ends can form linear chains, in solution chlorine or hydroxyl terminated polydimethylsiloxane or polydimethylsiloxane rings. At a hydrated silica surface treated with a DMDCS vapour, most of these chains start and end at a surface silanol group [42]. Only a small number of reactive ends remains at the surface. These chains can bridge surface areas without silanol groups, so that a better surface coverage with methyl groups is achieved. Although these chains are only chemically bound to the surface at their ends, vacuum stability has been shown [34]. A disadvantage is that these chains can grow randomly over each other, giving the risk of local structures which scatter the light.

MTCS can form heavily cross linked three dimensional polysiloxane networks in solution. At a hydrated silica surface treated with a MTCS vapour, no polymerisation of the MTCSs takes place [43], but already polymerised MTCSs can chemically bind to the surface. So with a controlled amount of water the degree of the polymerisation of the MTCSs adsorbed to the surface can be determined and thereby the surface area covered with methyl groups. The disadvantage here are the resulting three dimensional structures at the surface of the OMF, leading to an increased scattering of the light.

By using DMDCS or MTCS, open reactive ends will remain on the surface after a vapour treatment. For example, an MTCS binding to an isolated silanol has two reactive ends left. These unreacted end groups of DMDCS and MTCS have to be deactivated in an additional endcapping step. In [43] it was shown that the endcapping of MTCS can be done at ambient temperatures with TMCS in vapour, using TEA in vapour as a promoter before, which leads to tree like structures. It is also possible to bridge the areas between two reactive ends of surface adsorbed MTCS with linear chains by using TEA vapour and then DMDCS vapour. The

disadvantage here is the risk of reactive ends pointing away from the surface, leading to an increased height of the resulting structures.

For an OMF in caesium vapour, it is not possible to determine in advance which of the methylchlorosilanes or their combinations is needed for the desired protection.

4.3.2 Cleaning pretreatment

A critical point before exposing a fused silica surface to a methylchlorosilane vapour is the cleaning of the surface. On chemically grown silica, such a pretreatment does not only have a cleaning effect, but also influences the number of hydroxylated surface silanol groups significantly [13]. For fused silica in our case, the pretreatment is a pure cleaning step with the purpose of removing adsorbed molecules and dust, leaving only the (hydroxylated) silanol groups and some water layer on the surface. With such a clean and hydrated fused silica surface, reliable and repeatable results of the silylation can be achieved.

For cleaning our OMFs, the different materials connected to it have to be considered, namely the UV curing glue, the aluminium alloy of the holder and the acrylic coating at the fibre ends. To avoid a damage of these materials and unwanted reaction products during the cleaning procedure, only the fused silica surface of the OMF should be treated with the aggressive cleaning procedure needed.

In general, three standard procedures are used for cleaning silica surfaces. Baking out the silica in a vacuum chamber is not suitable for our situation due to the high temperatures needed. A plasma treatment with oxygen, hydrogen or water plasma could be in general applicable with the plasma localised to the OMF, but the technique needed was not available for me during this work. The procedure I decided to use is the cleaning of the OMF in a so called piranha solution. The term piranha solution is used for cleaning solutions with different recipes. The mixture I used consists of one part hydrogen peroxide (H_2O_2), 37 weight % in H_2O, and three parts sulphuric acid (H_2SO_4), 95 %. In the following, I will refer to this mixture as piranha solution.

Piranha solution is a very strong oxidiser, which has to be freshly made before each use. To avoid heavy reactions at the surface of an OMF, which lead to increased localised stress, and to reduce the risk of burning in some of the surface adsorbed contaminations, the fused silica surface is precleaned by rinsing it with various solvents. After the piranha cleaning,

the fused silica surfaces are rinsed with water to remove residual piranha solution and to be sure that the surface is hydrated.

The resulting clean silica surface is very hydrophilic due to the bare, reactive silanol groups (see section 1.3). The adsorption of molecules from the environment is greatly increased compared to the surface before cleaning.

Only glass, PTFE and to some degree certain stainless steel types withstand piranha solution and should be used for handling it.

4.3.3 Experimental procedure

The experimental procedures for the vapour treatments are adapted from [42][43]. For a first test of the implementation, I silylated fused silica mirror substrates from Altechna. Although the exact chemical surface properties among different samples of fused silica may vary, the treated fused silica mirror substrates are expected to be comparable to the surface of a treated OMF in basic points such as the occurrence and stability of a treatment effect and relative differences of the surface properties due to treatments with different methylchlorosilanes.

The solvents used for rinsing the fused silica mirror substrates were all HPLC grade. The TMCS was from Aldrich, purified by redistillation, purity $\geq 99.0\,\%$, the DMDCS from Dow Corning, purity $\geq 99.50\,\%$, the MTCS from Aldrich, purity $\geq 98.5\,\%$ and the TEA from Sigma-Aldrich, purissimum pro analysi, purity $\geq 99.5\,\%$. Handling of the silane liquids and the TEA was done under nitrogen (see below) using standard disposable syringes and stainless steel cannulas. The laboratory glassware used for all treatments is made of Schott Duran. For manipulating the mirror substrates, a pair of PTFE tweezers was used.

Nitrogen flowbox

Methylchlorosilanes react heavily with the water in the air (hydroxylation and polymerisation in solution, see section 4.3.1). Thus, their handling and the vapour treatment has to be done under a protection atmosphere. I used nitrogen as a protection gas because it was readily available.

All chemical treatments have to be done under a laboratory fume hood. The dust in the chemical room with the laboratory fume hood under which I worked is not filtered out from the air. Placing an OMF with its protection

44

cover removed under the laboratory fume hood exposes the OMF to a constant flow of air in which the normal amount of dust particles is contained. These dust particles adsorb to the surface of the OMF and lead to a complete transmission loss within minutes.

To provide a dust free nitrogen protection atmosphere, I built a nitrogen flowbox, figure 4.5.

For the nitrogen flowbox I made a frame out of aluminium profiles to which I screwed transparent polymethylmethacrylate (PMMA) plates with foamed EPDM as a sealing. In the front plate, two holes for handling inside the box were cut out, which can be closed if needed. One plate is fixed with two hinges to the aluminium frame and can be used as a gate. The size of the box is about (width x height x depth) 60 cm x 60 cm x 40 cm.

The nitrogen gas is led from the central liquid nitrogen tank to the chemistry room by metal pipes. For the connection from the metal pipes to the nitrogen flowbox, I first used hoses out of some rubber like material. During the treatments of OMFs, it turned out that these hoses had a significant outgassing. Not piranha cleaned OMFs exposed to the polluted nitrogen flow lost their transmission after about two hours due to a homogeneous coating with light absorbing or scattering molecules. With OMFs cleaned in piranha solution, the transmission was lost after about thirty minutes due to the increased adsorption of the molecules (see section 4.3.2). This coating could be removed and the transmission recovered by thoroughly rinsing the fibre with methanol, indicating physically or electrostatically adsorbed molecules.

The exact influence of this coating on the silylation is not known, but there is the risk that some silanol groups are not reached by the methylchlorosilanes or that the time the silica surface needs to to be exposed to the mehylchlorosilane vapour for all silanol groups being deactivated is increased by an unknown span. Furthermore, from the required monitoring of the transmission of an OMF during the treatments (see section 4.4) no statements about the influence of the treatments on the transmission can be deduced.

After an exchange of the tubings with low density polyethylene (LDPE) tubings, the coating effect on the OMFs was reduced, but did not vanish completely. Therefore, I exchanged all nitrogen tubings with polyamide tubings (PA 12, shore hardness D65) and used tubing connections out of hard polyamide (Serto Flip) or copper. Prior to assembling all tubings, connections and the exhausting silencers (see below), they were rinsed with acetone and flushed with nitrogen for three days. With this new nitrogen supply system, no coating effect of the OMFs could be observed.
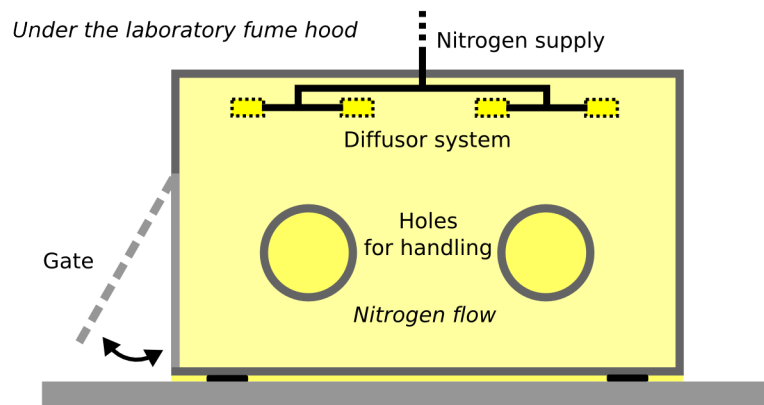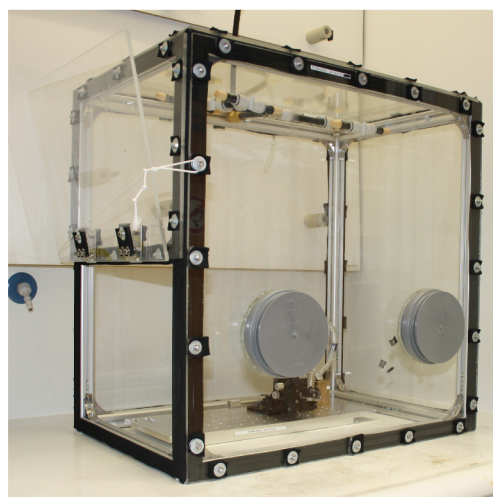
(a)
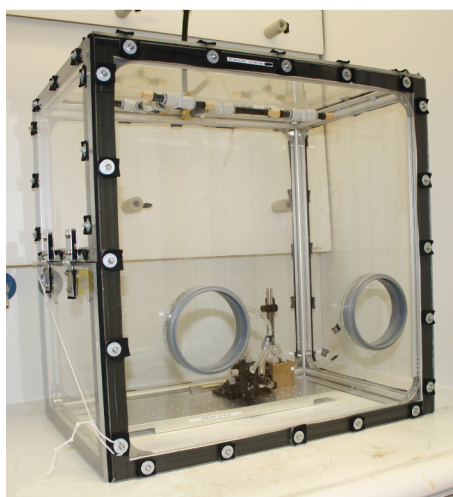
(b)   (c)

Figure 4.5: Nitrogen flowbox under the laboratory fume hood: (a) schematic sketch, (b) picture of the flowbox with the gate closed and the handling holes opened, (c) picture of the flowbox with the gate opened and the handling holes closed.

The treatments of the fused silica mirror substrates were done with the initial tubing in the polluted nitrogen. I could not repeat them with the

current nitrogen supply system because I did not have the time left. But assuming that the above mentioned coating did not improve the treatment effects, general conclusions about the success of the treatment procedure can still be made.

For the diffusor system, I mounted eight exhausting silencers made of sintered bronze equally distributed under the top plate. The silencers do not only reduce vibrations and noise caused by the high nitrogen flow needed, they also give an approximately laminar nitrogen flow about 20 cm below them.

The nitrogen can leave the box through the handling holes, the opened gate and a slit of about 2 mm between the box and the table underneath, so that dust and air are constantly blown out.

All treatments were done in the nitrogen flowbox.

Cleaning

The fused silica mirror substrates were first rinsed thoroughly with toluene, acetone, isopropanol, ethanol, methanol, water and methanol and dried under the nitrogen.

The piranha solution was prepared in a beaker outside of the nitrogen flowbox and transferred to it after the first heavy outgassing, usually after about five minutes. Then the substrates were laid in the piranha solution in an upright position and left in there for 15 minutes. Afterwards they were flushed with water and methanol and dried in the nitrogen.

Vapour treatment

The vapour treatments were done in a crystallising dish (diameter 190 mm, height 90 mm) with a PTFE cover plate (see figure 4.11). The substrates were placed upright on a PTFE block to be at about half height. Then about 3 ml of the liquid silanes or the TEA were transferred to a small dish and the crystallising dish was closed with the PTFE plate. After 15 min, the cover was removed and the small dish with a rest of the liquid was placed outside of the flowbox for evaporation. The substrates were left in the open crystallising dish for 15 min, so that the vapour could be blown away by the nitrogen and some of the surface adsorbed molecules could evaporate.

Post-treatment

After a silane vapour treatment, the substrates were thoroughly rinsed with toluene, acetone, isopropanol, ethanol, methanol, water and methanol to remove unreacted silanes and HCl, and then dried under the nitrogen. After a treatment with TEA vapour, no post-treatment was done.

Vapour treatment sequences

According to [43], a promoter like TEA is needed to achieve a chemical binding of MTCS to the silica surface and for the endcapping of MTCS with TMCS, see section 4.3.1. But to be on the safe side, I used TEA as a promoter before every silane vapour treatment.

The vapour treatment sequences I used were TEA-TMCS, TEA-DMDCS-TEA-TMCS and TEA-MTCS-TEA-TMCS, see section 4.3.1.

4.3.4 Characterisation of the treated surfaces

To characterise the treatment effect on a surface, I measured the contact angles of water drops (HPLC grade) on the substrates (figure 4.6).

The contact angle of a water drop on a surface is a measure for the hydrophobicity of the surface. The hydrophobicity is not only determined by the chemical properties of the surface, but also by its structure. A rough surface can be more hydrophobic than a smooth one with the same chemical properties, because the water drop can rest on the peaks on a rough surface due to the surface tension of the water (lotus effect) [44]. The lower areas on the surface are not reached by the water drop and do not contribute to the resulting contact angle.

Thus, the contact angles can only be compared when measured on surfaces with an equal average roughness. The fused silica mirror substrates are from the same charge so that their average surface roughness is expected to be equal.

The substrates were laid on a post so that the surfaces were horizontally within about one degree. The drop was formed slowly with water from a pipette, allowed to rest for a few minutes and a picture was taken with a mounted camera. In an analysis of these pictures the angles were measured, the resulting contact angle was taken as the average of the two angles in one picture. It was possible to determine the angles from the pictures with $\pm 1°$.

The substrate in figure 4.6a was only rinsed with solvents as described in the cleaning part of section 4.3.3. The contact angle of about 40 ° thus represents the hydrophobicity of the substrates as received.
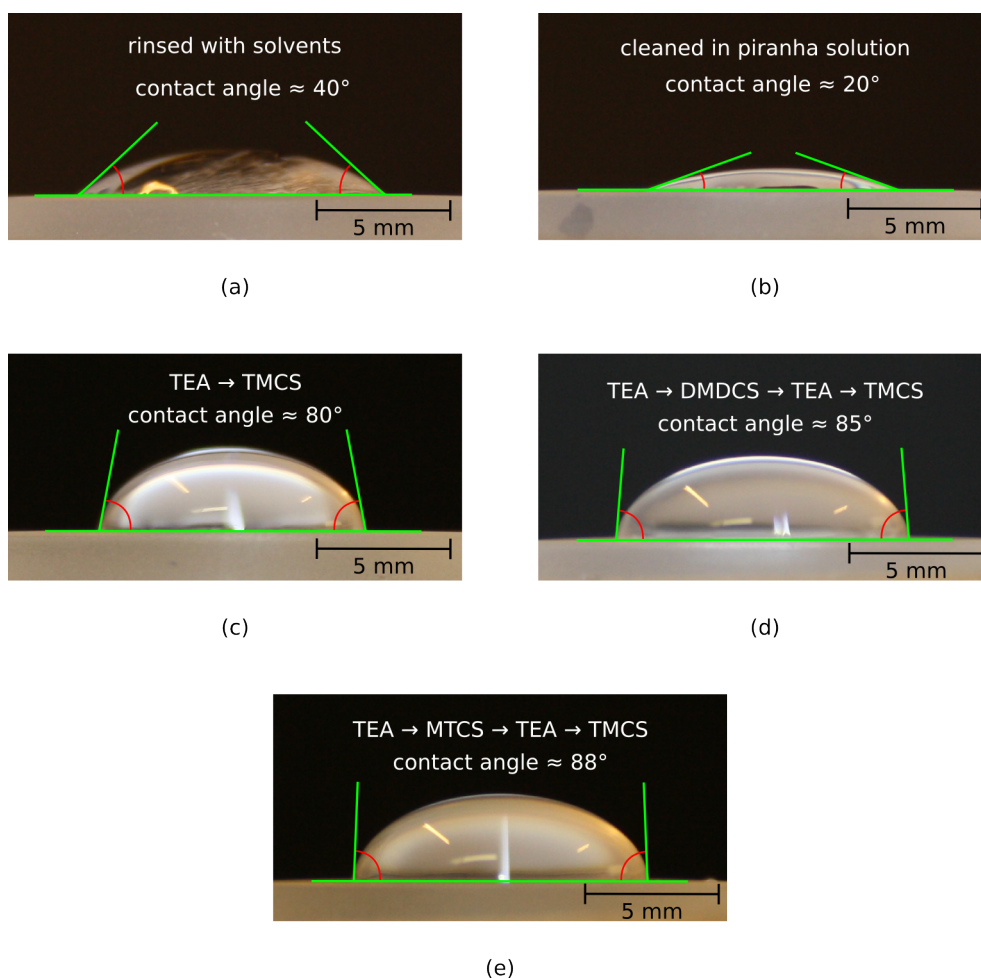

(a)

(b)

(c)

(d)

(e)

Figure 4.6: Contact angles of water drops on treated fused silica mirror substrates.

With a substrate additionally cleaned in piranha solution, the contact angles went down to about 20 ° (figure 4.6b) due to the removal of adsorbed molecules (see section 4.3.2). There might also be a minor rehydroxylation effect [13][7].

Before a first measurement of the contact angles of the methylchlorosilane treated substrates, the surfaces were rinsed with solvents as described in the post-treatment part of section 4.3.3. After a rinse with a solvent, they were additionally thoroughly wiped with lens tissues wetted with the last used solvent. A second measurement of the contact angles was taken after heating the substrates to about 60 ° for a day and repeating the rinsing and wiping procedure. The contact angles from both measurements did not show any measurable differences for each substrate. The pictures in figure 4.6c-e are from the second measurement.

With all three silane treatments the contact angles increased significantly. It can not be deduced from the rinsing, wiping and heating that this increase is due to actually chemically surface bound methylsilyls. But the measured contact angles and their stability are strong indications that the implementation of the procedure from [42][43] worked.

The larger contact angles for DMDCS and MTCS (figure 4.6d-e) are in agreement with the expected larger surface areas covered with methylsilyls compared to TMCS. For the MTCS treated substrate, their might also be an increased lotus effect contributing to the contact angle due the height of the structures formed by endcapping with TMCS, see section 4.3.1. This effect is not expected for the endcapped DMDCS because of the small number of reactive ends before endcapping [43].

4.4 Silylation of an optical microfibre: Procedure

Developing a procedure for cleaning and silylating an optical microfibre without destroying it required several attempts. After each of them there was the need of designing new mechanical parts, changing critical processes or redesigning central parts of the setup. In the following, I will present the working final procedure of the silylation of an OMF in a TMCS vapour with TEA vapour as a promoter.

Unless otherwise noted were all organic solvents used for this procedure UVASOL grade from Merck and the water was ROTIPURAN Low organic purity from Carl Roth. The TMCS was from Aldrich, purified by redistillation, purity $\geq 99.0\,\%$ and the TEA from Sigma-Aldrich, purissimum pro analysi, purity $\geq 99.5\,\%$. Handling of the silane liquids and the TEA was done under nitrogen in the flowbox using standard disposable syringes and stainless steel cannulas. The laboratory glassware used for all treatments is made of Schott Duran.

The nitrogen flow was initially adjusted to give a moderate flow through

the opened handling holes of the flowbox with the gate closed (see figure 4.5) and left on during the whole procedure.

During the development of the following procedure, no machine to fabricate an OMF was available, so that I had to use OMFs which we had in stock. To achieve transferable results for the silylation of an OMF for caesium spectroscopy, the OMFs needed to be destretched (see section 1.2), have waist diameters of about $0.4\mu\,m$ and their holder version had to allow the piranha cleaning, see below.

The OMF used for the following procedure fulfils these criteria, but was fabricated for a different purpose, see [2]. The waist and the tapers were pulled from a Newport F-SF single mode fibre (cutoff wavelength 660 nm – 800 nm), Nufern S630-HP (single mode, cutoff wavelength 560 nm – 620 nm) fibre ends were fusion spliced to it before the pulling process.

Preparation

Initially, the OMF in its holder with the protection cover was stored in a pink ESD bag (polyethylene, PE). It was inserted into the flowbox through the gate (see figure 4.5), unpacked and mounted to a goniometer - translation stage combination (figure 4.7a) with which an exact positioning of the OMF is possible.

The holder used for this OMF has slight modifications compared to the version in figure 1.2. It allows the lowering of the OMF into a liquid without wetting the holder, see the part about the piranha cleaning below.

The fibre ends were laid outside through the slit between the flowbox and the table and connected to a white light source (Ocean Optics LS-1) and a spectrometer (Avantes AvaSpec 3648-UA-25-AF). From here on, the transmission of the OMF was monitored continuously. All spectra were taken with 20 ms integration time and no averaging or smoothing. Below 400 nm and above 950 nm the transmission of the OMF was unstable, so that the spectra for these wavelengths are not shown.

The protection cover was removed and extensions were added to the holder (figure 4.7b). The fibre ends can brake easily at the gluing points with the aluminium protection cover removed. Due to the several required movements of the OMF in its holder during the treatment procedure, it is necessary to additionally fix the fibre ends behind the gluing points with aluminium extensions screwed to the holder. The original design of these extensions is presented in [1]. Due to the limited space in the crystallising dish (see below), I used extensions with a length of 15 mm.
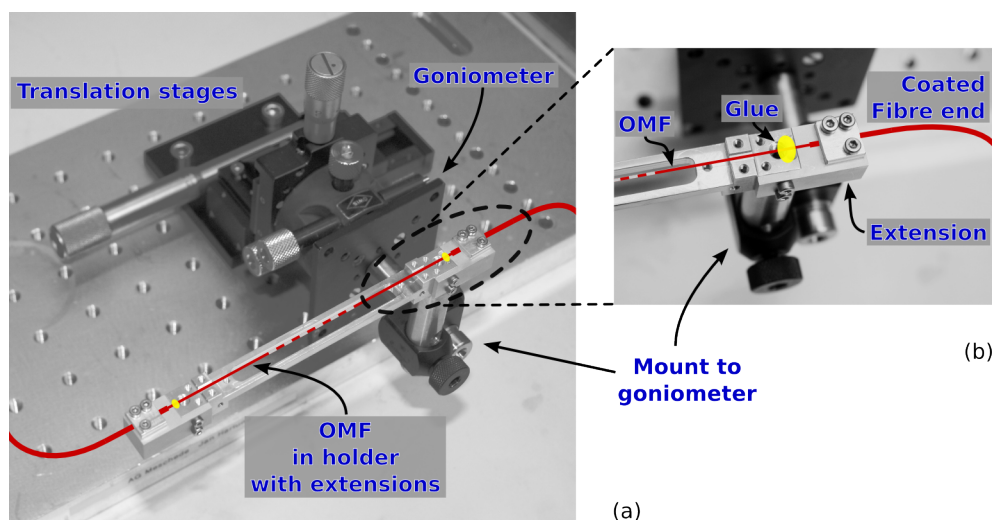
Figure 4.7: OMF in its holder with two extensions. The holder is mounted to a goniometer which is fixed to a translation stage combination. The mount to the goniometer allows turning the holder by 180 ° to have the OMF underneath it.

Cleaning: Rinsing

I rinsed the waist and the tapers of the OMF by letting drops of toluene, acetone, isopropanol, ethanol and methanol fall on them to remove as much of the adsorbed molecules and other contaminations as possible. Rinsing the OMF with pure water should be avoided. Due to the high surface tension of water, there are such high forces induced by the water drops to the OMF that the risk of ripping a waist with a diameter of about $0.4\,\mu\mathrm{m}$ is quite high.

The transmission monitored during the rinsing (figure 4.8) was taken as a feedback for the effect of each solvent. I rinsed the OMF with each solvent until no further transmission increase was observable.

After the rinsing, the OMF were allowed to dry in the nitrogen flow for about half an hour. The spectrum of the transmission after rinsing and drying is shown in figure 4.8. The dark and the reference spectrum for calculating the transmission were recorded before the rinsing.

For the smaller wavelengths a significant effect of the cleaning can be seen, indicating that a relevant amount of surface adsorbed molecules or dust particles were removed.
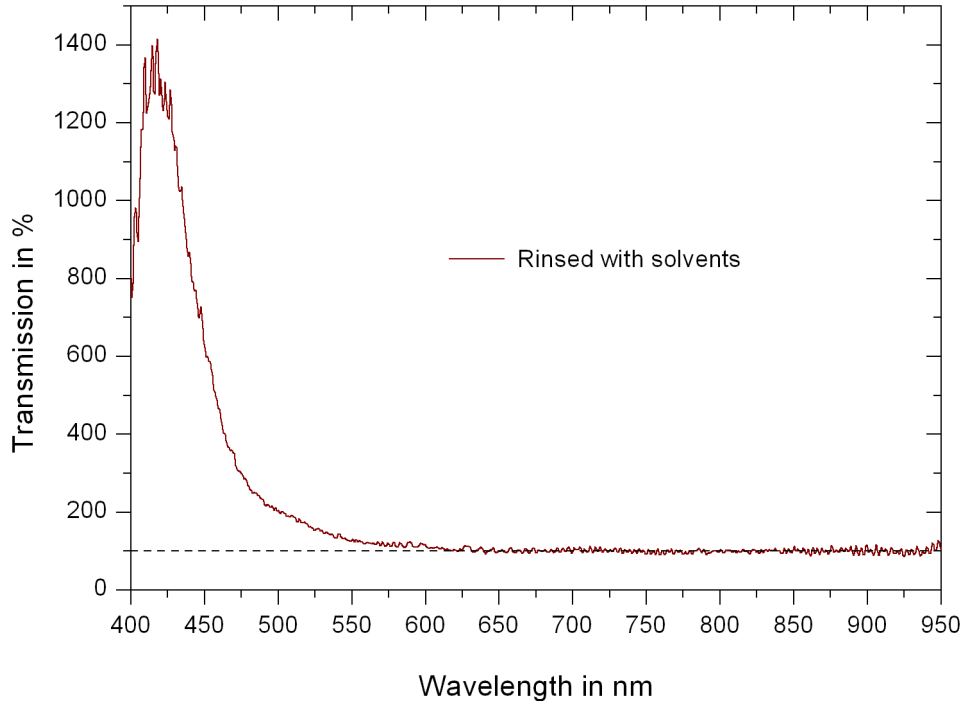
Figure 4.8: White light transmission of the OMF rinsed with various solvents and dried in nitrogen.

Cleaning: Piranha Cleaning

Cleaning the OMF with piranha solution turned out to be the most difficult part of the procedure. The goal is that at least the waist an the thin taper parts of an OMF stay about 15 minutes in the piranha solution. After this, the treated OMF parts have to be rinsed with water.

Because the piranha solution is a very strong oxidiser, it should only get in contact with the fused silica surface of the OMF. The UV curing glue (see section 1.2) and the acrylic coating of the fibre ends would be destroyed. An aluminium oxide layer on the holder would have a porous structure, leading to a decreased vacuum suitability.

The surface tension of the piranha solution is quite high and comparable to water. Therefore, piranha solution will form a high enough drop on a surface

into which the OMF can be lowered. The waist of an OMF with a diameter of about $0.4\mu m$ survives the lowering into such a drop, but not the raising out of it, the same holds for water drops.

By lowering the OMF into a piranha solution drop at a thicker taper part, moving it through the drop until the waist is in the drop, moving it back and raising the OMF out of the drop at a thicker taper part overcomes this problem. But the dried in residuals of the piranha solution on the waist lead to an almost complete loss of the transmission and can not be removed without destroying the OMF.

The principal of the piranha cleaning procedure that worked is the following. The OMF is lowered into a drop of piranha solution and left in there for 15 minutes. Water is then added to the drop so that the piranha solution is flushed away while the OMF stays in the drop. To raise the OMF out of the water, methanol is added to lower the surface tension. The setup is shown in figure 4.9a-b.

To get a well localised drop with the needed length (figure 4.9c), a certain reservoir for the piranha solution and the possibility to safely flush the piranha solution away with water, I designed a PTFE bath which was made by our precision mechanical workshop. In a PTFE block a U-shaped bath is cut (figure 4.9d). Piranha solution and water can extend above the bath by about 5 mm due to their surface tensions (figure 4.9c). Water added at one end of the bath will flush out the piranha solution, which flows out at the other end (figure 4.9d).

The bath is placed under the OMF in a stainless steel dish filled to about 10 mm with distilled water to dilute the flushed out piranha solution. After preparing the piranha solution outside of the flowbox in a beaker, it is transferred inside and carefully poured into the bath until it extends about 5 mm above the bath. The holder of the OMF is turned down, so that the OMF is underneath it. With the goniometer and the translation stages the OMF is positioned precisely over the bath to be parallel to the surface of the piranha solution and centred along it (figure 4.9b). Then it is lowered into the piranha solution and left in there for 15 minutes (figure 4.9a).
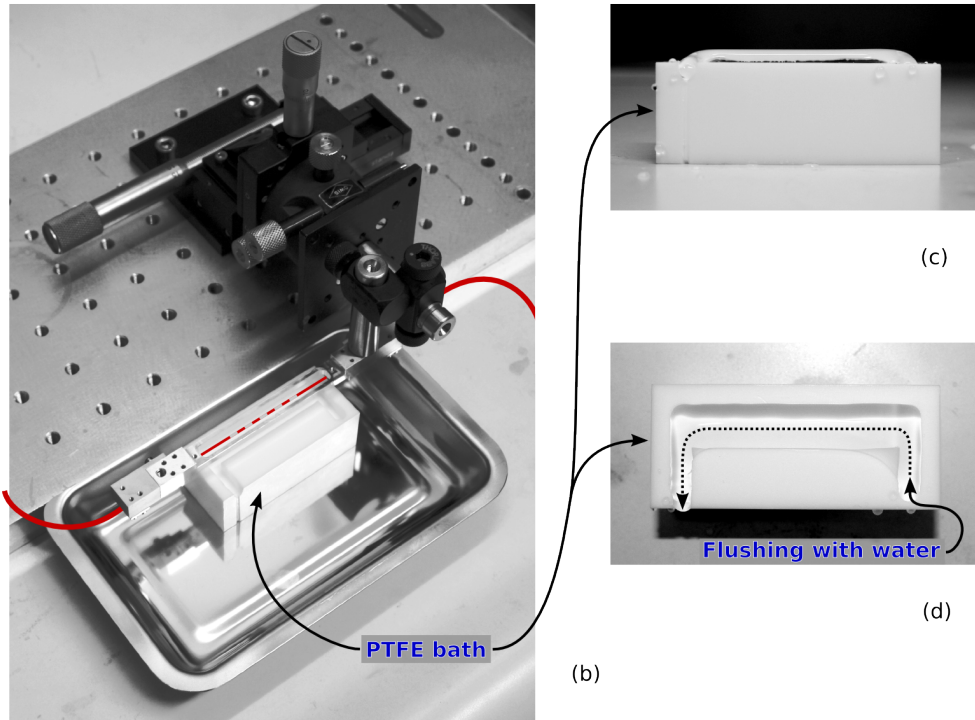
(a)

(b)

(c)

(d)
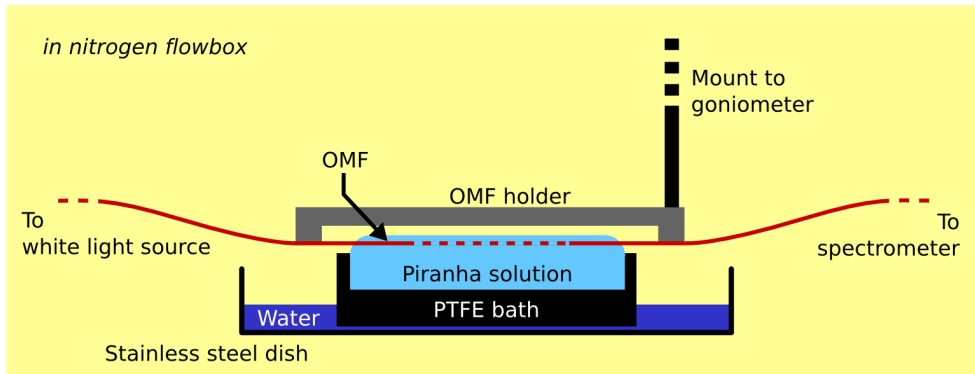
Figure 4.9: Setup for the piranha cleaning: (a) schematic sketch of the setup for the piranha solution, (b) picture of the setup, (c) picture of the PTFE bath from the side with water extending over it and (d) picture of the PTFE bath from above, showing the U-shaped cut out bath with the marked liquid flow while flushing with water.

The transmission went down to zero when the OMF was completely in the piranha solution (figure 4.10). For the spectra in figure 4.10, the dark and the reference spectra were recorded before beginning the piranha cleaning.
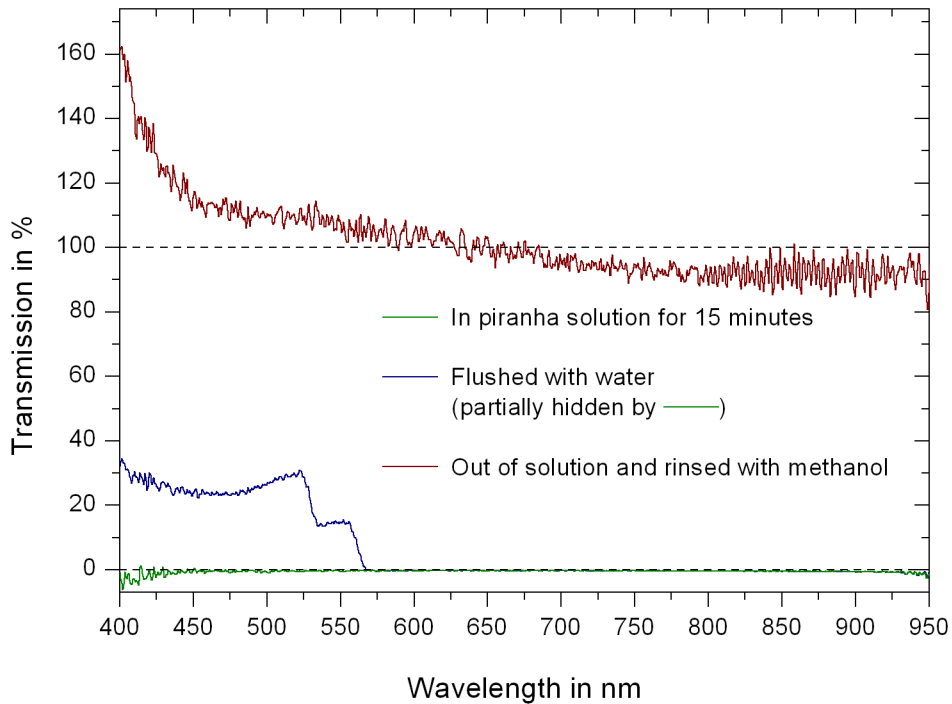

Figure 4.10: White light transmission of the OMF during piranha cleaning and after it.

The piranha solution was then flushed out of the bath with water. During this, the transmission increased below about 570 nm (figure 4.10). At some point the transmission did not change any more by further flushing with water, indicating that the piranha solution was flushed out completely.

Adding methanol drop wise to the water lowered the surface tension subsequently. The height of the fluid extending above the bath decreased until the OMF raised out of it. I rinsed the OMF with methanol to remove residual, not strongly bound water an let it dry in the nitrogen.

The transmission spectrum (figure 4.10) shows a further increase of the transmission at smaller wavelengths, indicating the removal of adsorbed

56

molecules or small dust particles. Above about 680 nm the transmission decreases to about 92 % for above 800 nm. This is only a minor decrease which can be caused by several reasons, like a change of the coupling to the white light source or the spectrometer due to the movement of the OMF holder during the treatment. Thus, the transmission of the OMF can at least be taken to have survived the piranha cleaning.

An interpretation of the spectra in the liquids is difficult due to the change of the optical properties of the OMF in them. In the piranha solution the formation of bubbles at the surface of the OMF due to the chemical reactions might be a reason for the complete transmission loss.

Vapour treatment: TEA

The vapour treatments were done in a crystallising dish with a PTFE cover plate. Due to the limited space inside the nitrogen flowbox, the breadboard with the goniometer - translation stage combination (figure 4.7 and 4.9) had to be taken out from the flowbox to put the crystallising dish inside. During this exchange the OMF was mounted to a post.

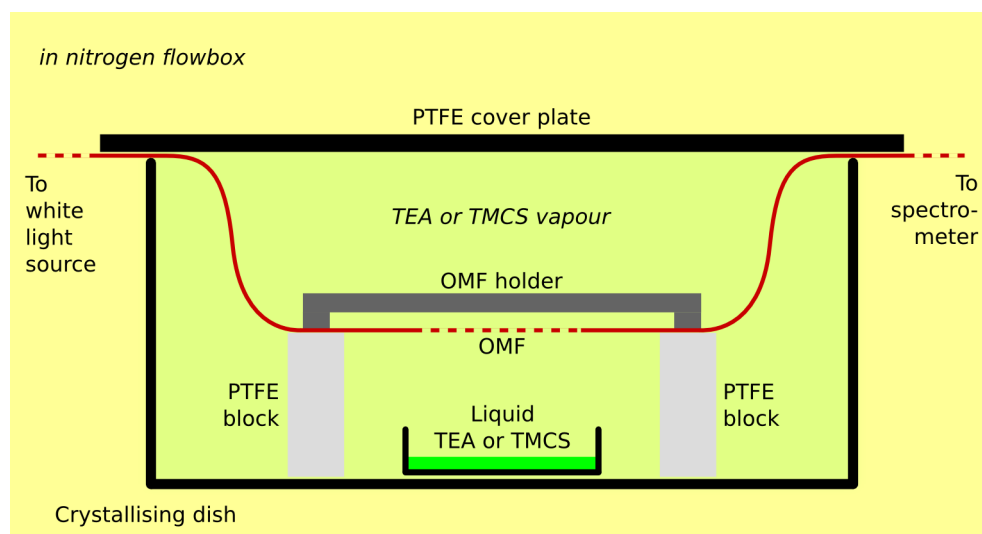In figure 4.11 the setup for the vapour treatment is sketched.

Figure 4.11: Sketch of the vapour treatment setup.

The holder of the OMF was placed on two PTFE blocks at about half

height of the crystallising dish. During the treatment with chlorosilanes, HCl is produced (see section 4.3.1) which attacks as hydrochloric acid the aluminium alloy of the holder. As a protection against acidic environments, some elements of the aluminium alloy travel to the surface and form there a black powder. HCl is heavier than the nitrogen and will concentrate in the lower part of the crystallising dish. But TEA and TMCS are also heavier than the nitrogen, so the half height is chosen as a compromise between avoiding the blackening of the OMF holder and exposing the OMF to a saturated vapour.

3 ml of the liquid TEA were transferred into a Petri dish and the crystallising dish was closed with a PTFE plate for 15 minutes. In figure 4.12 three spectra recorded during the exposure to the TEA vapour are shown.
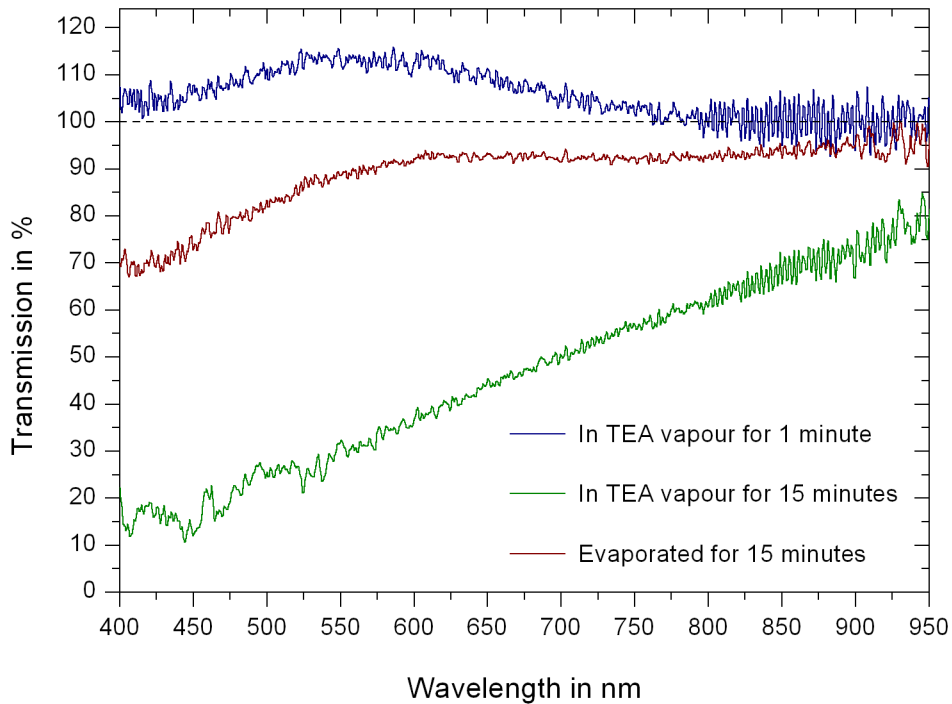
Figure 4.12: White light transmission of the OMF during exposure to TEA vapour and after evaporating.

The OMF was moved quite a lot between the piranha cleaning and placing it on the PTFE blocks. Due to the transmission changes induced by these movements by, for example, changes of the coupling to the white light source and the spectrometer or of the loss of higher modes in the fibre, the transmissions from before and after the movements are not comparable in detail. Thus, for the transmission spectra of the vapour treatments new dark and reference spectra were taken before starting the TEA vapour treatment.

Within the first minute of exposure to the TEA vapour the transmission increased below 800 nm. For the rest of the exposure, the transmission went down continuously leading to a almost linear shape of the transmission spectrum after 15 minutes.

After 15 minutes the cover plate was removed and the dish with the liquid rest of the TEA was placed outside of the flowbox. During evaporating, the transmission spectra jumped up and down in small steps with an overall significant increase of the transmission after 15 minutes.

The decrease of the transmission in the spectra after the first minute and the behaviour of the transmission spectra during evaporating indicate the macroscopic condensation of TEA on the OMF surface during the exposure. The light can scatter on small drops of TEA with a stronger effect on the transmission for smaller wavelengths. During evaporation, a combination of evaporating and recondensating TEA may have caused the jumps. The overall increase of the transmission after 15 minutes indicate the partial evaporating of condensed TEA. The origin of the increase of the transmission below 800 nm during the first minute is not known.

Vapour treatment: TMCS

3 ml of the liquid TMCS were transferred to a Petri dish (figure 4.11) and the crystallising dish was closed with the cover plate. The transmission of the OMF went down to zero within a few seconds (figure 4.13). For the spectra in 4.13, the same dark and reference spectra as for the TEA treatment were used.

After 15 minutes exposure to the TMCS vapour, the cover plate was removed and the dish with the liquid rest of TMCS was placed outside of the flowbox. During 15 minutes of evaporating the transmission of the OMF stayed zero.
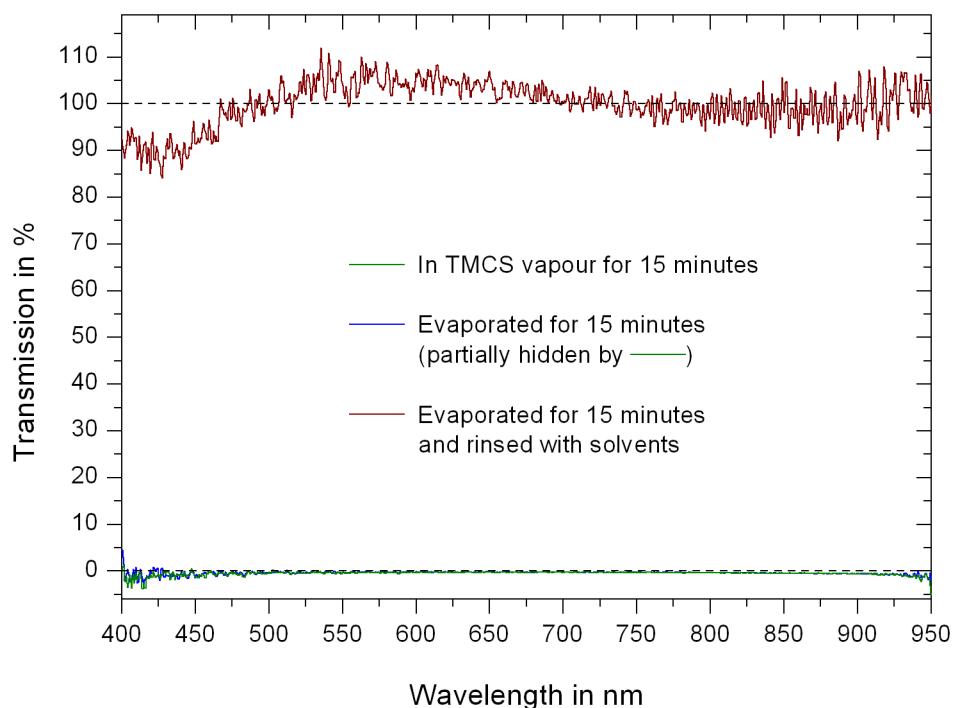
Figure 4.13: White light transmission of the OMF during exposure to TMCS vapour, after evaporating and additional rinsing with solvents.

The OMF was then rinsed with toluene, acetone, isopropanol, ethanol, methanol, methanol:water 1:1 and methanol. The methanol:water mixture was used because pure water may destroy the waist, see the rinsing section above and section 4.3.1. I rinsed the OMF with a solvent until no further change of the transmission spectrum was observable. Toluene and acetone showed hardly any effect, methanol had the strongest transmission increasing effect. The resulting transmission spectrum (figure 4.13) shows an almost 100 % transmission above about 680 nm. Below this wavelength, the shape of the spectrum is similar to the one of the spectrum after the TEA treatment.

The fast loss of the transmission in the TMCS vapour is probably caused by macroscopically condensed TMCS and HCl from the chemical reaction

of TMCS with the fused silica surface, see section 4.3.1. An evaporation effect after the vapour exposure could not be observed, indicating a quite strong physical binding of the molecules. By rinsing the OMF the transmission could be recovered almost completely. According to section 4.3, the fused silica surface of the OMF is now chemically deactivated with trimethylsilyl groups chemically bound to the former silanol groups, see section 4.3.1.

Summary

With the described procedure the OMF was successfully piranha cleaned and silylated with TMCS without a significant transmission loss. The surface of the OMF was chemically passivated and the optical properties of the OMF were conserved.

For a detailed interpretation of the monitored spectra (figures 4.10, 4.12 and 4.13) further investigations have to be done. But the transmission spectra of the OMF could be taken as a feedback for several important treatment steps of the presented procedure, like rinsing the OMF, flushing out the piranha solution with water and evaporating after the TEA treatment.

Due to the shortage of time I could not passivate further OMFs. But there are no general problems left in the presented procedure which would prevent the success of the treatment of another OMF.

5 Conclusion and Outlook

I have presented the optical setup for pump‑probe spectroscopy of hot atomic caesium vapour using optical microfibres. The special demands arising from the use of optical microfibres and the fibre system have been fulfilled. The first experiments with optical microfibres in hot caesium vapour have shown that the optical setup is working and ready to use.

The fast transmission loss of the optical microfibres in the caesium vapour prevented further experiments and led to the decision to protect the surface of our optical microfibres against chemical reactions with the caesium atoms. I have chosen to silylate the surface of optical microfibres with small methylchlorosilanes, because this method fulfils the numerous demands on an optical microfibre with a chemically passivated surface in hot atomic caesium vapour.

Therefore, I developed a procedure for piranha cleaning and silylating an optical microfibre. It has been shown in chapter 4 that with the presented procedure the surface of an optical microfibre was passivated and that the optical properties were maintained. Due to the shortage of time, no further investigations could be done. But there are no general problems left, so that further successful silylations can be done with the presented procedure.

The effect of the different proposed silylations has to be tested with a silylated optical microfibre in the hot caesium vapour, for which I did not have the time left. But it is expected that the silylation leads to significant increase of the time an optical microfibre can be used for spectroscopy in the caesium vapour.

With the optical setup I built and an optical microfibre with a passivated surface, saturated absorption and polarisation spectroscopy of the caesium vapour can be done to study the system optical microfibre - caesium atoms, for example transit time and surface effects.

The transit time effects include transit time broadening and a velocity selection, the surface effects van der Waals shift and surface induced anisotropy. With the polarisation spectroscopy, the anisotropy of the caesium atoms can be measured Doppler free and without a transit time broadening of the signals.

By applying an amplitude modulation to the pump beam, atomic adsorption and desorption dynamics at the surface of the waist can be studied, for example relaxation processes and light induced atomic desorption [45][30].

The addition of a light source with a wavelength far away from the wavelength of the diode laser gives the possibility of cleaning the waist with

light while recording spectra [29][1].

With a second, frequency locked laser, effects like electromagnetically induced transparency can be studied.

For the developed chemical treatment procedure, a characterisation of the treated and not treated surface of optical microfibres offers the possibility of improvement. Surface characterisation techniques, like infrared spectroscopy and scanning microscope imaging, could provide useful information about the surface properties of our optical microfibres before and after passivation.

References

[1] S. F. Bruse, "Harmonic Generation with Optical Microfibres under Controlled Atmospheres," Diploma thesis, University of Bonn, 2011, available at http://quantum-technologies.iap.uni-bonn.de.

[2] U. Wiedemann, "Control of photochromic molecules adsorbed to optical microfibres," PhD thesis, University of Bonn, 2011, available at http://quantum-technologies.iap.uni-bonn.de.

[3] G. Brambilla and V. Finazzi, "Ultra-low-loss optical fiber nanotapers," *Optics Express*, vol. 12, no. 10, pp. 2258-63, 2004.

[4] J. Love and W. Henry, "Quantifying loss minimisation in single-mode fibre tapers," *Electronics Letters*, pp. 912-914, 1986.

[5] M. Sumetsky, "Optics of tunneling from adiabatic nanotapers," *Optics letters*, vol. 31, no. 23, pp. 3420-2, 2006.

[6] F. Warken, "Ultradünne Glasfasern als Werkzeug zur Kopplung von Licht und Materie," PhD thesis, University of Bonn, 2007, available at http://quantum-technologies.iap.uni-bonn.de.

[7] R. K. Iler, *The chemistry of silica*. New York, John Wiley & Sons, 1979.

[8] M. Hair and W. Hertl, "Adsorption on hydroxylated silica surfaces," *The Journal of Physical Chemistry*, vol. 99, no. 12, 1969.

[9] L. T. Zhuravlev, "The surface chemistry of amorphous silica. Zhuravlev model," *Colloids and Surfaces A: Physicochemical and*, vol. 173, no. 1–3, pp. 1-38, 2000.

[10] L. Zhuravlev, "Concentration of hydroxyl groups on the surface of amorphous silicas," *Langmuir*, pp. 316-318, 1987.

[11] A. S. D'Souza and C. G. Pantano, "Mechanisms for silanol formation on amorphous silica fracture surfaces," *Journal of the American Ceramic*, vol. 82, no. 5, pp. 1289–1293, 1999.

[12] Y. Dong, S. Pappu, and Z. Xu, "Detection of local density distribution of isolated silanol groups on planar silica surfaces using nonlinear optical molecular probes," *Analytical Chemistry*, vol. 70, no. 22, pp. 4730-4735, 1998.

[13] V. Dugas and Y. Chevalier, "Surface hydroxylation and silane grafting on fumed and thermal silica.," *Journal of colloid and interface science*, vol. 264, no. 2, pp. 354-61, Aug. 2003.

[14] D. A. Steck, "Cesium D line data," Available online at http://steck.us/alkalidata (revision 2.1.4, 23 December 2010).

[15] D. Meschede, *Optik, Licht und Laser*. Wiesbaden, Vieweg + Teubner, 2008.

[16] S. Bagayev and V. Chebotayev, "Saturated Absorption Lineshape under the Transit-Time Conditions," *Laser Physics*, vol. 4, no. 2, pp. 224–292, 1994.

[17] S. Spillane et al., "Observation of nonlinear optical interactions of ultralow levels of light in a tapered optical nanofiber embedded in a hot rubidium vapor," *Physical review*, vol. 100, no. 23, pp. 1-4, 2008.

[18] M. Chevrollier, D. Bloch, and G. Rahmat, "Van der Waals-induced spectral distortions in selective-reflection spectroscopy of Cs vapor: the strong atom-surface interaction regime," *Optics letters*, vol. 16, no. 23, pp. 1879–1881, 1991.

[19] O. Schmidt, K. Knaak, R. Wynands, and D. Meschede, "Cesium saturation spectroscopy revisited: How to reverse peaks and observe narrow resonances," *Applied Physics B: Lasers*, vol. 59, no. 2, pp. 167-178, 1994.

[20] M. Harris, C. Adams, S. Cornish, I. McLeod, E. Tarleton, and I. Hughes, "Polarization spectroscopy in rubidium and cesium," *Physical Review A*, vol. 73, no. 6, pp. 1-8, 2006.

[21] L. Ricci et al., "A compact grating-stabilized diode laser system for atomic physics," *Optics*, vol. 117, no. 5–6, pp. 541-549, 1995.

[22] W. Alt, "Optical control of single neutral atoms," PhD thesis, University of Bonn, 2004, available at http://quantum-technologies.iap.uni-bonn.de.

[23] I. Kaminow, "Polarization in optical fibers," *Quantum Electronics, IEEE Journal of*, vol. 17, no. 1, pp. 15-22, 1981.

[24] R. Ulrich, S. Rashleigh, and W. Eickhoff, "Bending-induced birefringence in single-mode fibers," *Optics letters*, vol. 5, no. 6, pp. 273-5, 1980.

[25] R. Ulrich and A. Simon, "Polarization optics of twisted single-mode fibers," *Applied optics*, vol. 18, no. 13, pp. 2241-51, 1979.

[26] H. Storoy and K. Johannessen, "Glue induced birefringence in surface mounted optical fibres," *Electronics Letters*, vol. 33, no. 9, pp. 800–801, 1997.

[27] A. Smith, "Birefringence induced by bends and twists in single-mode optical fiber," *Applied Optics*, vol. 19, no. 15, pp. 2606-11, 1980.

[28] G. VanWiggeren and R. Roy, "Transmission of linearly polarized light through a single-mode fiber with random fluctuations of birefringence," *Applied optics*, vol. 38, no. 18, pp. 3888-92, 1999.

[29] S. Hendrickson, T. Pittman, and J. Franson, "Nonlinear transmission through a tapered fiber in rubidium vapor," *JOSA B*, vol. 26, no. 2, pp. 267–271, 2009.

[30] A. Burchianti, A. Bogi, C. Marinelli, and E. Mariotti, "Light-induced atomic desorption and related phenomena," *Physica Scripta*, vol. T135, p. 014012, 2009.

[31] F. Xu and G. Brambilla, "Embedding optical microfiber coil resonators in Teflon," *Optics letters*, vol. 32, no. 15, pp. 2164-6, 2007.

[32] Y. Wang and M. Liebermann, "Growth of ultrasmooth octadecyltrichlorosilane self-assembled monolayers on SiO2," *Langmuir*, vol. 19, no. 4, pp. 1159–1167, 2003.

[33] L. Zhuravlev, "Structurally bound water and surface characterization of amorphous silica," *Pure Appl. Chem*, vol. 61, no. 11, pp. 1969-1976, 1989.

[34] M. Stephens, R. Rhodes, and C. Wieman, "Study of wall coatings for vapor-cell laser traps," *Journal of applied physics*, vol. 76, no. 6, p. 3479, 1994.

[35] M. V. Balabas et al., "High quality anti-relaxation coating material for alkali atom vapor cells.," *Optics express*, vol. 18, no. 6, pp. 5825-30, 2010.

[36] S. J. Seltzer, D. M. Rampulla, S. Rivillon-Amy, Y. J. Chabal, S. L. Bernasek, and M. V. Romalis, "Testing the effect of surface coatings on alkali atom polarization lifetimes," *Journal of Applied Physics*, vol. 104, no. 10, p. 103116, 2008.

[37] M. Graf et al., "Relaxation of atomic polarization in paraffin-coated cesium vapor cells," *Physical Review A*, vol. 72, no. 2, pp. 25-28, 2005.

[38] C. Tripp, P. Kazmaier, and M. L. Hair, "A low frequency infrared and ab initio study of the reaction of trichlorosilane with silica," *Langmuir*, vol. 7463, no. 12, pp. 6404-6406, 1996.

[39] C. Tripp and M. Hair, "Reaction of chloromethylsilanes with silica: a low-frequency infrared study," *Langmuir*, vol. 7, no. 5, pp. 923–927, 1991.

[40] D. C. Fenimore, C. M. Davis, J. H. Whitford, and C. A. Harrington, "Vapor phase silylation of laboratory glassware," *Analytical*, vol. 48, no. 14, pp. 2289–2290, 1976.

[41] P. Silberzan, L. Leger, D. Ausserre, and J. J. Benattar, "Silanation of silica surfaces. A new method of constructing pure or mixed monolayers," *Langmuir*, no. 8, pp. 1647-1651, 1991.

[42] C. Tripp and M. L. Hair, "Reaction of methylsilanols with hydrated silica surfaces: the hydrolysis of trichloro-, dichloro-, and monochloromethylsilanes and the effects of curing," *Langmuir*, no. 13, pp. 149-155, 1995.

[43] C. Tripp and M. Hair, "Chemical attachment of chlorosilanes to silica: a two-step amine-promoted reaction," *The Journal of Physical Chemistry*, vol. 97, no. 21, pp. 5693-5698, 1993.

[44] W. Chen, A. Y. Fadeev, M. C. Hsieh, D. Öner, J. Youngblood, and T. J. McCarthy, "Ultrahydrophobic and ultralyophobic surfaces: some comments and examples," *Langmuir*, vol. 15, no. 10, pp. 3395–3399, 1999.

[45] H. D. Freitas, M. Oria, and M. Chevrollier, "Spectroscopy of cesium atoms adsorbing and desorbing at a dielectric surface," *Applied Physics B: Lasers and*, vol. 75, no. 6–7, pp. 703-709, 2002.

Erklärung

Ich versichere, dass ich diese Arbeit selbstständig verfasst und keine anderen als die angegebenen Quellen und Hilfsmittel benutzt sowie die Zitate kenntlich gemacht habe.

Referent: Prof. Dr. D. Meschede
Korreferent: Prof. Dr. M. Sokolowski